

AD615390

COPY	<u>2</u>	OF	<u>3</u>	<u>71-0</u>
HARD COPY	\$ . 3.00			
MICROFICHE	\$ . 0.75			

DNC  
MAY 14 1965  
ISA B

CLEARINGHOUSE FOR FEDERAL SCIENTIFIC AND TECHNICAL INFORMATION, CFSTI  
INPUT SECTION 410.11

*AD 615390*

LIMITATIONS IN REPRODUCTION QUALITY OF TECHNICAL ABSTRACT BULLETIN  
DOCUMENTS, DEFENSE DOCUMENTATION CENTER (DDC)

- ☐ 1. AVAILABLE ONLY FOR REFERENCE USE AT DDC FIELD SERVICES.  
COPY IS NOT AVAILABLE FOR PUBLIC SALE.
- ☒ 2. AVAILABLE COPY WILL NOT PERMIT FULLY LEGIBLE REPRODUCTION.  
REPRODUCTION WILL BE MADE IF REQUESTED BY USERS OF DDC.
  - ☒ A. COPY IS AVAILABLE FOR PUBLIC SALE.
  - ☐ B. COPY IS NOT AVAILABLE FOR PUBLIC SALE.
- ☐ 3. LIMITED NUMBER OF COPIES CONTAINING COLOR OTHER THAN BLACK  
AND WHITE ARE AVAILABLE UNTIL STOCK IS EXHAUSTED. REPRODUCTIONS  
WILL BE MADE IN BLACK AND WHITE ONLY.

TSL-121-2 65

DATE PROCESSED:

PROCESSOR:

LOCKHEED MISSILES AND SPACE COMPANY  
A Group Division of Lockheed Aircraft Corporation

TM 55-12-09

TM 55-12-09

SUMMARY REPORT - GASDYNAMIC  
INTERACTIONS  
INDEPENDENT DEVELOPMENT PROGRAM (U)

January 1965

WRITTEN BY: *V. V. Baicher*  
V. V. Baicher  
Internal Gas Dynamics  
Organization 55-12

*E. J. Kraus*  
E. J. Kraus  
Internal Gas Dynamics  
Organization 55-12

*H. A. Ashby*  
H. A. Ashby  
Internal Gas Dynamics  
Organization 55-12

APPROVED: *J. Hinzinger*  
J. Hinzinger  
Internal Gas Dynamics  
Organization 55-12

APPROVED: *J. E. May*  
J. E. May, Manager  
Internal Gas Dynamics  
Organization 55-12

SUMMARY

A seven-month study was conducted with \$95,000 of 1964 Augmented Independent Development Funds to determine the fundamental nature of the gas dynamic recirculation process which gives rise to staging force, moment, and environment problems in nearly all rocket powered separations. Parametric cold gas experiments were conducted for a series of progressively more complex idealized interstage configurations which would exhibit, in sequence, the steps in the recirculation phenomenon. Theoretical work was initiated which is expected to lead to a method for making preliminary design estimates of recirculation effects on a wide variety of potential vehicle staging configurations.

The experimental program was completed in full, with sufficient force, pressure, and photographic data taken on all the planned configurations to support theoretical analysis. Plotted pressure and force data taken on the majority of the experimental configurations is presented in an Appendix. Some of the data is not included due to lack of time for reduction and plotting. A comparison between certain of the data and previous experimental results is made, showing good agreement.

A discussion of theoretical concepts concerning interstage gas dynamics is given, in which a scheme for calculating recirculation is envisioned as an iteration procedure, involving a series of independent stagnations and intervening supersonic re-accelerations within the interstage. Examination of the data shows such a step-wise process of stagnations to exist, and thus the envisioned procedure appears feasible, providing each of the independent steps can be correctly calculated.

Theoretical analysis was completed on the first stagnation process in the sequence of steps leading to recirculation, and a preliminary method for the second stagnation within the interstage was devised. However, the first stagnation method was found to be inadequate within a high pressure interstage environment, when it was compared

to the experimental data toward the end of the project. The remaining time was devoted to studying how this method could be corrected and what implications could be drawn concerning the interstage calculation as a whole. The inadequacies of the theory in the interstage environment are examined by comparing various modifications of the theory to the experimental data. The method of predicting the separation rocket jet boundary appears inadequate, with no better method available which is also sufficiently rapid for the computerized interstage application. The assumption of zero mass and momentum flux in the jet boundary region appears poor. While the proper value can easily be assigned to jet boundary strength, the interaction of the jet boundary of this strength, with flow attempting to leave the first stagnation region appears to invalidate the boundary conditions for the stagnation assumed in the theory. However, under experimental conditions where the jet boundary is very weak, the first stagnation theory does show reasonable agreement with experiment, implying that the basic equations of the theory are valid.

From the comparisons of theory and experiment it is found that the interaction of the jet boundary with the first stagnation flow field produces a thin gas layer along the floor of the interstage. Thus it is concluded that interstage vents located at floor level would be particularly effective in reducing recirculation for single-stage rocket powered separation designs. Likewise, sealing the region of each interstage floor, in a design involving simultaneous rocket separation of several adjacent stages, may be expected to greatly reduce recirculation between the stages.

TABLE OF CONTENTS

SUMMARY	1
LIST OF TABLES AND FIGURES	iv
LIST OF SYMBOLS	v
INTRODUCTION	
Nature of the Recirculation Problem	1
Importance of Recirculation to Vehicle Designs	2
Expected Future Occurrence of Recirculation	3
Available Methods and Data for Recirculation Problems	3
Objectives of the Independent Development Study	4
PROJECT PLAN	
Original Plan and Funding	6
Fulfillment of Project Plan	7
DESCRIPTION OF EXPERIMENTAL WORK	
Model Description	8
Test Conditions	9
Instrumentation	10
Data Acquisition	11
Test Summary	11
EXPERIMENTAL RESULTS	
Data Reduction	13
Description of Experimental Data	14
Data Validity	14
DESCRIPTION OF THEORETICAL WORK	
Introduction	16
First Stagnation Theory	17
COMPARISON OF FIRST STAGNATION THEORY AND EXPERIMENT	
Experimental Data Used	19
Comparison of Theory and Experiment	20
Investigation of the Assumptions of the Theory	22
IMPLICATIONS OF THE THEORETICAL - EXPERIMENTAL COMPARISONS	26
CONCLUSIONS	

LIST OF TABLES AND FIGURES

Table I	Sonic Nozzle Test Summary	30
Table II	Supersonic Nozzle Test Summary	31
Table III	Adjacent Jet Simulating Fence - Sonic Nozzle	32
Figure 1	Nature of Recirculation	33
Figure 2	Sequence of Test and Analysis Configurations	34
Figure 3	Test Setup - Schematic	35
Figure 4	Nozzle Details	36
Figure 5	Model Configurations - Schematic	37
Figure 6	Nomenclature	39
Figure 7	Adjacent Jet Simulating Configuration	40
Figure 8	First Stagnation Nomenclature	41
Figure 9	Comparison of Theory and Experiment - Case 1	42
Figure 10	Comparison of Theory and Experiment - Case 2	43
Figure 11	Comparison of Theory and Experiment - Case 3	44
Figure 12	Comparison of Jet Boundary Approximations	45
Figure 13	Comparison of Theory and Experiment - Case 4	46
Figure 14	Comparison of Results	47

# LIST OF SYMBOLS

<u>Symbol</u>	<u>Explanation</u>
A	Cross-sectional area (area in x-r plane) - radii <sup>2</sup>
B	Height of pressure top on experimental splitter fence from interstage floor plate - radii
C	Nozzle mass or momentum constant (see Appendix I)
F	Height of pressure top on experimental circular fence from bottom of fence - radii
f	Radial distance from experimental nozzle centerline to splitter fence, measured normal to fence - radii
H	Height of pitot probe from interstage floor plate - radii
h	Height of bottom of experimental circular fence from interstage floor plate - radii
K	Stagnation layer area error sensitivity constant (see Appendix I)
M	Mach number of gas flow
m	Sides of wedge-shaped control volume, V.
$\dot{m}$	Flux of mass - slugs/sec.
P	Pressure - lbs/in <sup>2</sup>
R	Radial distance from nozzle-plate centerline to an experimental pressure top - radii
r	Radial distance from nozzle centerline - radii
s	A point on the interstage floor shock
T	Thrust parameter - lb.
V	First stagnation control volume, bounded by the floor shock, the wedge sides (m), the interstage floor, and the layer exit (d) - see Figure (8)
$V_1$	Volume occupied by jet flow between nozzle and interstage floor shock - see Figure (8)
x	Axial distance from nozzle exit - radii
$\alpha$	Flow angle measured from jet axis - degrees



<u>Symbol</u>	<u>Explanation</u>
$\beta$	Angle of tilt of experimental nozzle-jet axis from plate - container axis - degrees
$\sigma$	Separation rocket exhaust ratio of specific heats
$\delta$	Distance of standoff from the interstage floor surface radii
$\Delta x$	Width of first stagnation layer measured in the x direction - radii
$\nu$	Prandtl - Meyer angle - degrees
$\psi$	Angle between pitot probe axis and the plane perpendicular to experimental interstage plate - container axis - degrees
$\rho$	Radius of the spherical jet boundary or floor shock approximations - radii
$\sigma$	Angle between a line of experimental pressure taps and a line from the nozzle centerline perpendicular to a splitter fence, measured positive counter-clockwise looking toward nozzle - degrees
$\theta$	Angle between sides (m) of first stagnation control volume (V) - see Figure (8)
$\phi$	Angle between jet axis and perpendicular to the interstage floor shock - degrees
$\Omega$	Angle between a line of experimental pressure taps and the positive right-hand vector direction of nozzle tilts ( $\beta$ ), measured clockwise looking at nozzle - degrees

<u>Subscript</u>	<u>Explanation</u>
a	in the ambient air or in the interstage cavity
assumed	value assumed at the start of an iteration
b	at the separation rocket jet boundary
c	at the separation rocket jet centerline, or referring to mass flow from nozzle
calculated	value computed at the end of an iteration
d	at the exit of the first stagnation layer
f	at a point on the interstage floor
in	into a volume

<u>Subscript</u>	<u>Explanation</u>
j	at a point in the separation rocket free jet
l	at a point in the first stagnation layer
n	at the separation rocket nozzle exit
NP	at a point on the experimental nozzle plate
o	between the jet and experimental plate - container centerline at the level of the plate
out	out of a volume
P	at a point on the experimental interstage floor plate
R	at a point on an experimental pitot - tube rake
r	in the jet radial direction.
T	Total or stagnation value in a flow
x	in the jet axial direction, or referring to flux of axial momentum from nozzle
*	at the nozzle throat

## INTRODUCTION

### Nature of the Recirculation Problem

Recirculation flow, causing gas dynamic interactions between separating vehicle stages, is common when staging is at high altitude and the separating stage is powered by a rocket motor which is ignited during the staging sequence. Under these conditions the jet wake from the rocket motor, expanding to the low ambient pressure, may fill the space between the stages and stagnate directly on the floor of the interstage volume. When this occurs (Figure 1) a strong peak in floor pressure is set up where the jet flow is normal to the surface, with pressure declining rapidly away from the peak in all directions. These floor pressure gradients cause the stagnating flow to re-accelerate to supersonic speeds laterally along the floor surface away from the peak. A second stagnation may take place with supersonic flow recirculating up toward the separating stage, if there is any interstage hardware blocking lateral escape of gas (Figure 1a), or if there is an adjacent jet stagnation flow field opposing the lateral flow of gas from under the separating stage (Figure 1b). Recirculation is the existence of any supersonic reverse flow directed back onto the separating stage, which arises from the deflection of exhaust gas from the stage's own rocket motor.

Although there may be substantial gas dynamic interactions between the stages, recirculation does not occur during fire-in-the-hole separation (initially closed interstage), such as Polaris first separation. This is because a high pressure is rapidly achieved in the interstage volume which confines the separation rocket jet wake and suppresses supersonic stagnations and re-expansions. Supersonic recirculation flow gradually becomes important as more and more venting is allowed in the interstage design, provided the separation occurs at high altitude, so that ambient pressure does not confine the flow in the interstage. Because the interstage pressure must be high to suppress recirculation, fire-in-the-hole separations are characterized by higher staging forces than separations in which recirculation predominates.

However, when recirculation is present, in a vented design, staging forces may be much higher than would be expected assuming complete mixing within the interstage for that design. This is because the momentum of the reverse flow jet is available to act on the separating stage, in addition to the interstage cavity pressure, and for supersonic reverse flow, this momentum may be quite large.

#### Importance of Recirculation to Vehicle Designs

The presence of supersonic recirculation flow within an interstage usually poses serious vehicle design and performance problems. Often the principle problem is the large force produced on the separating stage base by the stagnation of the reverse flow jet. The axial component of this force imparts an unexpected velocity to the separating stage, changing its trajectory. If the separating stage is unguided, no in-flight correction can be made for this velocity change. Even in guided stages, the velocity perturbation often occurs in too short a time to be sensed accurately by the guidance system. This often results in vehicle accuracy problems. For example, the recirculation occurring during separation of the unguided A3 re-entry system shifts the point of impact down range by approximately six miles.

Because the recirculation flow is supersonic, the pressures it produces on both stages may be unsymmetrical, imparting angular rates to the stages. This occurs if the interstage hardware is unsymmetrical, or if adjacent separating stages have different ignition times or different thrust levels. Angular rates during staging may cause clearance problems, and if the stages are unguided, their trajectories will be affected. For example, the position, orientation, and radar cross section of the Polaris A3 re-entry system components have been drastically affected by recirculation-induced angular rates, and during re-entry, these rates cause re-entry body limit-cycle wobbling oscillations which increase radar scattering by the wake.

Finally, important design problems are often caused by unexpectedly high structural loads and heating produced in the interstage by the recirculation flow field. For

example, the high loads experienced on the Polaris A3 forward heat shield, during re-entry body separation, have required about 50 lb. of extra structure in this area. Even so, the smaller components (firing units, cables, snubbers, etc.) are regularly torn off the missile by the recirculation flow field and scattered about the sky. This has greatly complicated the problem of radar data analysis from test flights.

#### Expected Future Occurrence of Recirculation

Recirculation problems during re-entry system separation on the Polaris A3 will continue to be important as the system undergoes modifications. Even minor changes, such as different instrumentation layouts in test flights, have been observed to change the recirculation effects substantially. Large changes, such as envisioned for the Mark XII adaptation, will probably introduce completely new recirculation problems. Supersonic flow in the interstage which has been shown to occur during B3 first stage separation (Reference a) must also be solved.

Recirculation effects should be anticipated in any highly vented interstage design, such as envisioned in various large solid booster concepts. For example, interstage recirculation gas dynamics produce important problems in the highly-vented Saturn interstage (Reference b). Recirculation forces, and debris carried by the recirculation flow field, may be important during lunar landing and take-off (Reference c), especially if there is substantially irregularity in the landing surface.

#### Available Methods and Data for Recirculation Problems

The flow in the expanding jet from the separation rocket nozzle may be calculated by the LMSC method-of-characteristics computer program of Reference (d). A Newtonian approximation to the interstage floor pressures, produced by the direct stagnation of this jet, may be calculated with the jet impingement computer program of Reference (e). However, these pressures may be substantially in error if a recirculation flow field

exists between the free-jet flow and the interstage floor surface. When the interstage is initially closed (fire-in-the-hole), so that recirculation is suppressed, a computer program assuming complete mixing, Reference (f), may be used to calculate the axial force during separation. However, this method gives no information on local flow conditions within the interstage. Also, it shows poor agreement with experiment when the separation plane is near the interstage floor, or where venting is initially present near the floor. When recirculation flow is responsible for the staging forces, there is no analytical method for predicting magnitudes or determining local flow conditions over interstage hardware.

Large amounts of experimental data on Polaris A3 re-entry body separation forces and interstage pressures have been accumulated at LMSC (References (g), (h), and (i)). These data are for reasonably exact scale models of different re-entry system designs, and consequently the geometries are very complicated. Further, pressure data are very limited, with no pitot tube or other surveys of recirculation flow conditions. Considerable interstage static pressure and vent flow pitot pressure data have been taken on the separation of a small body from a highly vented container (Reference j), in which the vents are longitudinal and not axisymmetric, and the interstage floor may have a shape which varies with time in a complicated way. Reference (b) contains interstage floor pressure data for designs with similar vents to those of Reference (j), and various (fixed) floor shapes. There are no flow property surveys in Reference (b). Reference (k) presents pressure data on a flat plate due to the impingement of various jets at low ambient pressures, and gives Schlieren photographs showing jet boundaries and stagnation shock shapes.

#### Objectives of the Independent Development Study

Although attempts have been made to develop analytical methods for predicting recirculation effects, using the available experimental data (especially that of Reference i), the complications of the configurations tested have proved insurmountable. To develop

an analytical capability, consideration of simple configurations is necessary, with subsequent generalizations to more complicated designs. However, no experimental data exists on simple interstages, with which to verify a theoretical analysis (except for Reference (k) in which there is no interstage at all). The importance of recirculation estimates in the design of advanced Polaris re-entry systems, and the lack of fundamental theoretical knowledge about recirculation, led to the present study on 1964 Augmented Independent Development Funds, to develop a basic understanding of the recirculation process.

The objectives of the Gas Dynamics Interactions study were:

- 1) To develop an analytical method for computing recirculation staging forces for simple designs in which the interstage is symmetric about the separation rocket nozzle axis.
- 2) To generalize the axisymmetric method to various idealized types of asymmetries found in actual vehicle designs.
- 3) To accumulate parametric experimental data on recirculation flow field properties and induced staging forces, for idealized axisymmetric and non-axisymmetric designs, and use these data to assist in the development of the theory and provide information on trends which could be used in design estimates.

Because of the emphasis on idealized configuration in both the theoretical and experimental investigations, this work was supported by Independent Development Funds. By divorcing the study from any specific vehicle design, it was hoped the results would apply to preliminary design estimates for many different types of vehicles.

## PROJECT PLAN

### Original Plan and Funding

Theoretical analysis was planned for a series of progressively more complicated axisymmetric interstage designs, beginning with the first stagnation of the separation rocket jet on plates representing interstage floors of various shapes, then proceeding to add the sides and top of the interstage, and to consider various types of venting (see Figure 2). Generalization of the axisymmetric method was to be attempted for inclination of the separating stage from the interstage axis, and for the presence of adjacent separating stages assumed to be identical to the stage under consideration. Experimental data was to be taken on each of the idealized configurations considered in the analysis, so as to support and verify each step of the theory. Sufficient pressure distributions, flow field property surveys, and photographs of flow field structures were to be taken to permit thorough checkout of the assumptions made in the theoretical work.

The plan called for testing to begin as soon as possible after approval of the project. To accumulate large amounts of data quickly and at low cost, cold-flow testing was planned for LMSC's Tenney Altitude Chamber (84-33). Design and fabrication of the simple axisymmetric model configurations was scheduled to be complete by mid-August, with the first data to be available for analysis by the end of August. Testing of more complicated models was to continue to the end of the project.

The development of a theoretical method for computing recirculation forces in the axisymmetric design was planned to begin before the testing, and to be complete by the end of October, allowing two months for the use of test data in this effort. Generalization of the axisymmetric method to the various asymmetries was to begin in November and to continue concurrent with testing of the corresponding configurations.

The total budget for the project was \$95,000. Of this amount, 55% was allocated to engineering work on the theory, data correlations, model design, and test conduct.



Approximately 30% of the budget was to be used for facility charges and data reduction computer programming. 15% of the budget was for model fabrication.

#### Fulfillment of Project Plan

The objectives of the experimental phase were met in full. Testing was completed on all the configurations planned, with several configurations and conditions tested which were not originally scheduled. Adequate pressure surveys, loads and photographic data were obtained to permit theoretical analysis of all the configurations. However, the start of testing was delayed to the end of September because of lack of personnel available at the beginning of the project, problems with facility scheduling, and problems with the photographic setup. The first data were not available for analysis until the beginning of November. The test schedule was very much compressed to finish the planned testing within allocated funding. Consequently, much data was accumulated with very little concurrent analysis of the results.

The theoretical analysis of the first stagnation of the separation rocket jet on the interstage floor was completed by the end of August, and results from an RPC 4000 computer program were obtained by the end of September. Calculation of further flow re-accelerations and stagnations within the axisymmetric interstage had been studied, and an RPC 4000 program had been drawn up by the end of October. With the availability of experimental data in November, it was found that the First Stagnation program failed to agree with experiment for many cases of interest. The remaining analysis time was spent in studying the data to determine why the First Stagnation theory was failing, how it could be corrected, and what implications could be drawn concerning the interstage calculation as a whole. No progress was made on the calculation of the various non-axisymmetric test configurations.

## DESCRIPTION OF EXPERIMENTAL WORK

### Model Description

The test was conducted at the LMSC Tenney Altitude Facility during the period September-October 1964. A schematic of the test set up is presented in Figure (3). High pressure nitrogen gas from 12 standard commercial bottles, manifolded in parallel, flowed through a valve and out through a nozzle onto a plate or into a vented container within the evacuated test chamber. Thrust produced by the nozzle and the force acting on the plate were measured using load cells. Pressures measured included ambient (test chamber) pressure, nozzle chamber pressure, static pressures on the plate and on the walls of the containers, and pitot pressures in the jet wake and in the vent areas. High speed Schlieren motion pictures were taken during most runs. The axial distance between the nozzle and the plate and the container vent area were varied from run to run.

To facilitate completing the test schedule within the allotted time, the test set-up was planned for maximum convenience of operation. Nitrogen pressure regulation, valve control, and camera frame rate and on-off control were accomplished outside the test chamber. The separation distance between the nozzle and all the various plates or containers was remotely controlled using an electric motor to drive a worm and wheel gear arrangement.

Two different nozzles were used during the test program: a sonic nozzle and a supersonic nozzle having an expansion ratio of 5.5 to 1. These nozzles are shown in Figure (4).

As shown in Figure (5), interstage floor configurations tested included a flat plate, and a conical plate. Certain model configurations included a flat plate concentric with the nozzle axis and mounted in the plane of the nozzle exit (nozzle plate). Several runs were made with the nozzle tilted with respect to the plate-container axis. A circular fence two inches high and four inches in radius mounted concentrically about the nozzle axis, was used with the flat plate to simulate a vented container into which the

jet exhausted. The fence was moved axially between the plate and the nozzle to furnish different vent areas. The circular fence was also used with the nozzle plate to simulate a re-entry body flare. The effect of adjacent jets was simulated using a flat plate and splitter fences (see Figure 5). The presence of two, three, and six jets was thus simulated.

The parameters that were varied from run to run (see Figures 6 and 7) included the separation distance between the plate and the nozzle exit plane ( $x$ ), the distance from the plate to the bottom of the circular fence ( $h$ ), and the radial distance between the nozzle axis and the splitter fences ( $f$ ). The plate and the fences were attached so that they had the same movement relative to the nozzle exit plane.

On-off control of the nitrogen flow was through a solenoid controlled, hydraulically actuated quick opening Jamesbury ball valve. Constant nitrogen pressure during a run was maintained with a dome regulator.

#### Test Conditions

Before every test was run the Tenney Chamber was evacuated to a pressure altitude of approximately 117,000 feet. After a test run (each run lasted one second) the altitude had dropped to about 105,000 feet, an increase in test chamber pressure of about 65 percent. The nozzle chamber pressure averaged about 1450 psi during a run. This average chamber pressure varied from run to run, being dependent on the bottle pressure. Approximate extremes of average chamber pressure were 1350 psi and 1510 psi. Within a test run the chamber pressure reached operating level within 30 milliseconds after the valve was actuated and would drop approximately 50 psi per second in most cases. The speed at which nozzle pressure decreased (or increased) depended on the pressure in the bottles.

As shown in Figure (6), separation distance ( $x$ ) varied from  $10.7 r_n$  (nozzle exit radii)

to  $49.5 r_n$  when the sonic nozzle was used, and from  $4.153 r_n$  to  $19.25 r_n$  when the supersonic nozzle was used. Cylindrical fence height was 2" ( $21.7 r_n$  sonic,  $9.07 r_n$  supersonic). The distance from the plate to the bottom of the circular fence ( $h$ ) varied from 0 to  $21.7 r_n$  sonic and from 0 to  $4.53 r_n$  supersonic. Maximum lower vent area formed by this separation between plate and fence was  $7,840 A_t$  (nozzle throat area) for the single-stage configurations, and with the adjacent jet (splitter fence) models the maximum area was  $1960 A_t$ . Only the sonic nozzle was used with the splitter fences.

### Instrumentation

Instrumentation used in the test program included strain gage pressure transducers and load cells, a position transducer, thermo-couples, bourdon tube pressure gages for measuring nitrogen supply pressure, and a bourdon tube vacuum gage for measuring test chamber pressure.

Thrust produced by the nozzle, and the force produced by the jet impinging on the plate or container, were measured using single-bridge strain gage load cells.

Strain gage pressure transducers, of both absolute and differential types, were used to measure test chamber pressures and model pressures, including pitot pressures in the jet wake and in vent areas and static pressures on the plates and fences. Typical locations for these measurements are shown in Figure (6). A position transducer, the output of which was on digital display, was used to set the separation distance. Two thermocouples were used to measure temperatures in the shock layer on the plate. In addition to force and pressure instrumentation, extensive use was made of photographic instrumentation consisting of a modified schlieren system and a high speed motion picture camera. As shown in Figure (3), light from a point source was passed through the test model and returned to the camera lens along the same path by a 12" diameter aspheric mirror.

All load cells and pressure transducers were physically calibrated before their installation in the model. In this physical calibration the output of the transducer was read on a strain indicator. Also, with no load on the transducer, known resistances were shunted into the circuit, producing changes in the strain indicator reading. Thus, steps were obtained relating apparent load on the transducer with resistance in the circuit. These steps were shunted into the circuit to make the electrical transducer calibrations before each test run.

#### Data Acquisition

Analog signals from the strain gage load cells and pressure transducers were digitized and recorded by the Data Acquisition System (DAS) of O/84-33. A digitizer accepted analog input voltages from the transducers and load cells and derived a number proportional to the amplitude of each voltage at the time of sampling. This number (millivolts) was then written on magnetic tape in BCD format. Time identification was recorded with the test data. After each series of runs, the data was dumped onto cards and also listed by an IBM 407 accounting machine.

Before each test run, with the test chamber at the proper simulated altitude, no-load transducer outputs were recorded, then an electrical calibration made. In this electrical calibration a known resistance (the same as used in the pre-test physical calibration) was shunted into each transducer circuit, producing a change in millivolt counts in the DAS. This permitted deriving a relationship between load (force or pressure) on the transducer and electrical output in millivolt counts.

#### Test Summary

The test program required approximately ten weeks to complete, including three weeks for calibration and installation of transducers and set-up of the model and the nitrogen supply. During the seven weeks of testing, 259 runs were made, 167 with the sonic nozzle and 92 with the supersonic nozzle.

A complete summary of the experimental configurations may be found in Tables I, II and III. Table I summarizes the sonic nozzle configurations tested, while Table II presents the supersonic nozzle configurations. Table III summarizes the adjacent jet simulating fence configurations, all of which were tested with the sonic nozzle.

EXPERIMENTAL RESULTSData Reduction

To facilitate the reduction of the data, obtained as counts (see previous section), a 7094 Fortran data reduction computer program was written (Reference r). This program was designed to quantify and list the experimental data. The program converts as-received counts into data expressed in engineering units. This data is listed as a function of time, as is normalized data. Data is normalized to a nozzle source pressure of 1000 psia by dividing the data by the instantaneous average nozzle pressure and multiplying the result by 1000. In addition, the program permits calculation of average values of the data over a specified time interval, as well as generation of plots of any or all data versus time for the same time interval.

Due to the fact that some of the pressure transducers measured differential pressure, while others measured absolute, additional operations were performed on the reduced data to give all pressure measurements in absolute units. To obtain the absolute loading on both the flat plate and nozzle plate - nozzle combination, it was necessary to convert the differential force measured experimentally by adding the ambient pressure loads acting on the test-cell sides of the plates. The total normalized force in each case was then divided by the average normalized nozzle thrust taken from all the flat plate test runs.

The average nozzle thrust was used to determine the force/thrust ratio rather than the thrust for the test run in question, for two reasons. First, for runs which included the nozzle plate, the measured force on the nozzle plate included the pressure loading on the plate due to recirculation as well as the nozzle thrust. Since there was no way to accurately separate the two contributions to the force, the nozzle thrust for those runs was unknown. Second, a plot of nozzle total pressure versus measured thrust did not reveal the expected linear relationships. Since for a given nozzle, the thrust should be directly proportional to the nozzle total pressure, other, unknown effects made their presence felt. These effects may have included, for example, errors in

force measurement or nozzle flow problems, such as the effective half angle or exit Mach number differing from design conditions. The value of average thrust was 35.495 pounds for the sonic nozzle, and 41.487 pounds for the supersonic nozzle. Both of these figures are normalized to a nozzle total pressure of 1000 psia.

#### Description of Experimental Data

For purposes of presentation, the data was divided into three classifications as follows:

1. Sonic Nozzle Configurations
2. Supersonic Nozzle Configurations
3. Adjacent Jet Simulating Fence Configurations

A summary of the configurations tested can be found in Tables I/, II, and III.

Plots of the experimental test data for the first two classifications, sonic and supersonic nozzle configurations, may be found in Appendix II. The nozzle total pressure to ambient pressure ratio for the data presented in the appendix is, nominally, 12,000. In Appendix II plots of plate pressure distributions, nozzle plate pressure distributions, fence pressure distributions, plate force/thrust ratios vs separation distance, nozzle plate force/thrust ratios vs separation distance, and rake pressures vs separation distance, are presented. The photographic data on flow field structures is not presented due to lack of time available to scale and map the photographs to compensate for angle-of-view distortions (see Comparison of First Stagnation Theory to Experiment, for a discussion of the analysis required).

Due to time limitations, the data from the third classification, the adjacent jet simulating fence configurations, is not included in Appendix II. However, these data were reduced and rough plots made during the data analysis effort, so that the data are available for use in theoretical work and design estimation.

#### Data Validity

To assess the validity of the data, a comparison of the flat plate pressure distributions



from Appendix II with the experimental data of Reference (k), and with the theoretical predictions of the program of Reference (e) has been made in Figure (14).

For purposes of comparison, it was necessary to cross plot the experimental data of Stitt (Reference k) to obtain data at the same separation distances as were tested. Further, it should be noted that Stitt's data was obtained at a pressure ratio of  $1.52 \times 10^5$  while the present data holds for a ratio of  $1.2 \times 10^4$ . This difference affects the tails of the distribution, since the pressure ratio determines the boundary of the jet. The core region does not appear to be greatly affected by the ratio, however. It can be seen that the experimental data from the test and from Stitt are in good agreement.

The Newtonian jet impingement theory of Reference (e), compared in Figure (14), assumes the plate shock lies directly on the surface, with no standoff distance. This would be expected to give lower pressures on a flat plate than actually occur because the Mach number in the jet is higher at the plate than at any shock standoff distance above the plate. This is borne out in Figure (14), where jet impingement data is lower at the axis than either experimental data source. The magnitude of this difference is consistent with the standoff distance observed in the photographs of the test configurations.

## DESCRIPTION OF THEORETICAL WORK

### Introduction

As described under Project Plan, the theoretical studies were concentrated on a series of progressively more complicated axially symmetric interstage designs, beginning with the problem of a jet stagnating on a plate, then considering stagnations against the sides and top of the interstage. This organization stemmed from preliminary concepts concerning interstage recirculation gas dynamics drawn from jet impingement studies (e.g. Reference c) and the data of References (i) and (k). It appeared that the flow in the interstage, for recirculation cases, was a step-wise process of stagnations and re-accelerations, with each stagnation process separated from the preceding one by a supersonic region (see Figure 1a). Thus it was thought that each area of stagnation could be solved independently from the other areas, given only the interstage pressure, the interstage geometry, and the supersonic flow conditions upstream of the stagnation. By solving the stagnation of the jet on the plate to obtain the flow conditions leaving the stagnation layer, it was thought that the initial conditions would then be given for calculation of the acceleration of gas along the plate and stagnation against the interstage sides. Likewise, solution of the side stagnation was anticipated to set up the independent problem of the stagnation against the top of the interstage. A scheme for solving the axisymmetric interstage was envisioned in which interstage cavity pressure ( $P_q$  of Figure 1) would be first assumed, then the chain of stagnations and re-accelerations around the interstage would be calculated, and from the degree to which the mass flow out of the interstage found for the various exits was different from the mass flow in from the nozzle, a new interstage pressure would be assumed. The process would be repeated until the interstage was in balance. Thus, the theoretical analysis of the first stagnation of the separation rocket jet on a plate, given the plate shape and the surrounding ambient (or cavity) pressure, was considered as an independent problem, with application of the results to the re-acceleration and

side stagnation a separate study.

As has been indicated in Project Plan, the analysis of the first stagnation was completed, but based on assumptions which make the analysis inadequate in the high-pressure confined environment of the interstage. However, this method does show reasonable agreement with experiment in very low ambient pressure cases, and might be modifiable for high pressure cases. Consequently, a discussion of this work is given below. The analysis of the side stagnation was set up, but without good flow conditions predicted from the first stagnation within the interstage, the adequacy of the side stagnation theory could not be investigated. Theoretical work was done on first stagnation for the nozzle tilted with respect to the plate, but this study could not be carried far enough to produce results.

#### First Stagnation Theory

Two methods were investigated for calculating the normal stagnation of a jet on a concentric axisymmetric plate. A stream tube continuity approach along the lines suggested by Reference (m) was attempted, which would give the detailed flow field within the stagnation layer. Persistent mathematical difficulties were encountered and a working method was not completed. A second approach was to make a control-volume analysis of the layer (volume V of Figure 8), to determine the total load on the plate, the height of the layer at the jet boundary, and the average flow conditions crossing the exit of the layer (d of Figure 8). This method was considered adequate to solve the staging force problem and provide input flow conditions to the side stagnation calculation. A working method and an RPC 4000 computer program were developed using the control-volume analysis.

A full discussion of the control-volume method is given in Appendix I. The basic equations are conservation of mass, axial momentum, and radial momentum for volume V of Figure (8). These equations introduce (9) unknown quantities and thus (6)

additional relationships are required. The basic assumptions of the method are that the jet boundary is given by the circular arc method of Reference (n), the stagnation shock is a spherical cap, and only isentropic jet flow as given by the program of Reference (d) crosses the stagnation shock (i.e. the thickness and strength of the jet boundary region is negligible). The shock stand off distance on the jet centerline is taken from Reference (o). These assumptions permit relations to be drawn between the unknown layer exit height ( $\Delta x_d$  of Figure 8) and exit radius ( $r_d$ ), exit average flow angle ( $\alpha_d$ ), exit total pressure ( $p_{Td}$ ) radial momentum flux entering the layer, and layer cross-sectional area. The sixth relation is the assumption that average layer static pressure equals average plate pressure. With these relations, the three basic equations are solved by a double-iteration scheme. Typical results of the analysis are shown in Figures 9-11.

COMPARISON OF FIRST STAGNATION THEORY AND EXPERIMENTExperimental Data Used

To obtain sufficient data for a comparison to all the results of the theory, it was necessary to supplement the pressure and load measurements of Appendix II with data drawn from the schlieren photographs. The information obtained from these photographs was the location and the shape of the separation rocket jet boundary and the floor stagnation shock wave (see Figure 8). Assuming the flow in the expanding jet to be correctly given by the program of Reference (d), the flow conditions crossing d of Figure (8) at the shock (s) were calculated from the photographic shock angle. Flow along the interstage floor was calculated from the measured plate pressure distribution. Average flow conditions crossing d, for comparison to the theoretical average values, were taken as the average of the conditions at s and f.

For the experimental configurations having simply the nozzle and the flat plate, the jet boundary and the plate shock were generally completely visible in the photographs. However, the shock appeared to lie very close to the plate, or at times to disappear within the plate on the centerline. This was due to viewing the model with a cone of light produced by the slit source and returned by the aspheric mirror (Figure 3). The plate was thus viewed at an angle, and some of the stagnation layer was obscured behind the elliptical plate shadow. Although no correction was required for the photographic axial distances from the nozzle to points on the shock, the true position of the plate had to be determined from the known view angle and the photographic position of the rear edge of the plate. After this position had been determined, the axial scale of the photograph was calculated from the known and photographic separation distances.

For the configurations involving the circular fence, the fence often obscured most of the jet boundary and plate shock, except for the view through the region of the axis provided by a 1.5" x 2" plexiglass window. The analysis of the axial scale and hardware

positions was as above, except that both the nozzle and plate positions were obscured and required determination from the angles of view. The areas of the jet boundary blocked by the fence were filled in by noting the pressure to which the known flow in the jet was raised in crossing the visible boundary shock wave, and continuing this shock through the jet in such a way as to be a smooth curve and maintain the pressure behind it constant. The intersection of the plate shock with the boundary was determined from the derived boundary shape and the ring of interaction representing this intersection which was visible in the window.

#### Comparison of Theory and Experiment

The experimental data for three test configurations is compared to the first stagnation theory in Figures 9-11. Figures (9) and (10) refer to free jets, at a nozzle pressure ratio ( $P_{Tn}/P_a$ ) of 12,000, impinging on flat plates. Figure (11) is the jet impingement within an interstage configuration at a nozzle pressure ratio of 1130. All three cases involve the sonic nozzle of Figure (4). The solid lines are experimental values and the dashed lines are from the theory of Appendix I.

From these figures it is seen that there is excellent agreement between theoretical plate shock standoff distance on the jet centerline (taken from Reference 6) and the standoff measured from the photographs. As a consequence, there is good agreement between theoretical and experimental centerline plate pressures, which are governed by shock standoff. However, the theoretical jet boundary (as predicted by the circular arc method of Reference 6) deviates greatly to the outside of the photographic boundary. The radius of the stagnation layer exit ( $r_d$  of Figure 8) is thus much greater in theory than in experiment. The deviation of the various theoretical results from experimental values becomes difficult to interpret in view of the disparity in geometry, and the fundamental way in which  $r_d$  enters into the analysis (see Appendix I). It should be noted that theoretical plate load ( $L$ ), layer exit static pressure ( $P_d$ ), pitot pressure ( $P_{T2d}$ ), flow angle ( $\alpha_d$ ), and Mach number ( $M_d$ ) agree remarkably well

with the experimental values at the radius ( $r_d$ ) taken by the theory, even though the actual layer exit is not located there. However, the first stagnation theory of Appendix I must be regarded as unsuitable for use on the recirculation problem as long as it fails to predict the correct height and radius of the stagnation layer.

#### Investigation of Methods for the Jet Boundary

The method used to obtain the jet boundary is not fundamental to the analysis of the stagnation layer but an independent problem, since the expanding separation rocket jet is supersonic. The circular arc method of Reference (n) was chosen because of its speed, and because the comparisons to experiment in that reference were favorable. The need for speed in the boundary calculation for the interstage application arises because the cavity pressure surrounding the jet is not known a priori but is an iteration variable. Each iteration necessitates the calculation of a new jet boundary. Thus, if the boundary calculation is time consuming, the length of time necessary to completely solve one interstage problem could be prohibitive.

The method of characteristics has been shown to give boundaries which agree quite well with experiment (see Reference p). This method, which produces very accurate results, is, however, extremely time consuming. An example of the agreement between the program of Reference (d) and the present experimental data is shown by the calculated points in Figure (9).

In the interest of speed and ease of calculation, a number of approximate methods have been developed for boundary determinations including the circular arc method of Reference (n) adopted in the theory. Three methods are presented in Figure (12), compared to the method-of-characteristics boundary calculated for the case of Figure (11). Good agreement is seen for both the Latvala approximate method (also given in Reference n) and the Adamson and Nicholls method (Reference q) for small values of  $x/r_n$  (see inset,

Figure 12), with the Latvala method being slightly better. Both methods are more accurate in this region than the Latvala circular arc. However, both methods shortly cross over the characteristics solution and thence continually deviate in such a manner as to produce boundaries considerably in excess of the correct boundary and even in excess of the circular arc boundary.

The circular arc approximation could be much improved by decreasing the initial expansion angle. This decrease has no basis in theory, but a similar decrease was found advantageous by Latvala for similar pressure ratios (Reference n). At larger pressure ratios, the agreement further downstream still leaves much to be desired, being generally larger than the actual boundary, then curving too rapidly and cutting across the boundary.

It thus appears that none of these approximate methods are suitable for predicting the jet boundary a large number of exit radii downstream of the nozzle, which is the region of interest in the recirculation calculation. The only reliable method is the method of characteristics, which has the large disadvantage of being excessively time consuming. Either some concise tabulation of characteristics boundaries for the nozzle in question would have to be employed, or some new approximate method derived from characteristics theory would have to be developed, in order to permit the continuation of the first stagnation calculation and the solution to recirculation.

#### Investigation of the Assumptions of the Theory

To further investigate the assumptions of the first stagnation analysis, the theoretical jet boundary estimates were forced to agree with the photographic boundaries of Figures 9-11, by adjusting the boundary expansion angle at the nozzle, as suggested by Latvala, in Reference (n). The first-stagnation analysis was then repeated for these cases. The results are shown in Figures (9-11) by the dotted lines.

It is seen that the comparison between theoretical and experimental stagnation 1 per



geometry and flow properties is good only for Figure (9). The theoretical layer exit height ( $\Delta x_d$ ) becomes progressively greater than the experimental value in Figures (10) and (11). This deviation is believed due to the influence of the jet boundary. For the case of Figure (9), the ambient pressure is low and the length of boundary involved is fairly small, so that the boundary region (region between jet boundary shock and the interface with ambient air) is thin, and the strength of flow in this region is small. The assumption of the theory that the boundary is negligible appears good for this case. For the case of Figure (10), however, the boundary is apparently long enough to have captured a substantial amount of gas from the jet core. This boundary evidently prevents appreciable flow from entering the stagnation layer across the plate shock. Thus the theoretical method, which assumes all the jet gas to be involved in the layer, predicts appreciably too great a layer height. This situation is carried to extremes in Figure (11), where the high ambient pressure of the interstage produces a very thick and strong jet boundary. In fact, at the experimental layer exit point,  $s_d$ , (see Figure 8) over half the thrust of the jet is concentrated in the boundary. Under these circumstances, the assumption that the boundary is negligible, and that all the jet gas is contained in the isentropic core and crosses the plate shock, gives ridiculous results.

To further investigate the theoretical assumptions, the first stagnation method was applied to the case of Figure (11), with not only the jet boundary adjusted to agree with experiment, but with the axial momentum and mass flow considered to cross the plate shock ( $C_x$  and  $C_c$  of Appendix I) adjusted to the actual amounts contained in the jet core. The results are shown in Figure (11) by the dot-dash lines. The predicted layer geometry is seen to be very good, as is layer exit flow angle. However, the plate load is considerably lower in theory than in experiment, the theoretical layer exit Mach number ( $M_d$ ) is much too high and the exit static pressure ( $P_d$ ) is much too low. Since these results were not obtained in the adjusted-boundary calculation of Figure (9), they point to an influence of the relatively high-density boundary in

restraining the exit of flow from the layer, causing a build-up of pressure within the layer and on the plate. It appears that the calculation of first stagnation of the jet on the interstage floor cannot be made by ignoring the jet boundary and assuming the jet flow to be isentropic. In the high pressure interstage environment, the requirement that the high-density boundary stream be turned by the flow accelerating across the plate out of the stagnation layer, evidently imposes a different character to the layer from that to be expected in near-vacuum impingement. The presence of the jet boundary must be incorporated into the first stagnation theory before good results can be expected.

It should be noted from Figure (11) that the pressure gradient across the interstage floor is sufficiently great to induce supersonic flow between the first stagnation layer exit and the sides of the interstage. Thus, the first stagnation process is independent of the side stagnation process. Likewise, supersonic flow exists along the sides between the bottom and top of the interstage. It would seem that the assumption of a step-wise sequence of independent stagnations is correct, and that a theoretical method for recirculation which is based on this assumption would be feasible.

The question of how the high density jet boundary of Figure (11) (total pressure = 260 psi) interacts and is turned along the plate by the relatively low density stagnation layer flow (total pressure = 4 psi) is fundamental to an understanding of the conditions which would have to be incorporated into the first stagnation theory to make it correct. This question has been studied by a conservation analysis of the small volume shown in the inset, Figure (11), making use of the measured plate pressure distribution and assumed linear pressure and flow angle distributions across the flows. In this analysis, the boundary and layer flows have been assumed not to mix, but to retain their separate identities. Since the layer flow is subsonic, it has been assumed isentropic. The results, shown in Figure (11), are that the boundary flow turns, and

grows greatly in width, while losing total pressure rapidly. The layer flow continues to accelerate towards  $M = 1$ , and thus becomes smaller in thickness. The indication is that as flow continues to expand to greater radii, the boundary stream will continue to broaden, turn, and lose total pressure, occupying an ever increasing proportion of the ever decreasing total layer width. The method of turning the boundary must be through shocks induced in that stream by the subsonic layer flow underneath, and reflected expansions induced when these shocks strike the interface with ambient air. This process continues until the layer flow reaches  $M = 1$ , at which point shocks can propagate also through this stream and reflect from the plate. The hump in the plate pressure distribution of Figure (11) is very suggestive of such a process. The result is expected to be a rather thin, two-layered high density flow along the plate, with the boundary flow occupying most of the width.

One further observation on the theoretical assumptions arises from an attempt to apply the first stagnation theory to near-vacuum impingement on the cone-shaped experimental plate configuration. The method of Reference (o) predicted a centerline shock standoff distance much smaller than the experimental value. Using this distance, the calculations became mathematically unstable and no solution was found. The instabilities were of a type previously encountered in the development of the theory (see Appendix I), and are believed to be associated with insufficient stagnation layer cross-sectional area during iteration. With the small centerline standoff distance, the theory could not pass a spherical shock out the cone and achieve sufficient layer area at all points. This is shown in Figure (1)). Thus, the method of Reference (o) is not adequate to give centerline standoff distance when the interstage floor has a slope at the center. This is not surprising since the assumption that the plate surface near the jet centerline is normal to the centerline is fundamental to the analysis in Reference (o). That method would have to be generalized for sloped surfaces in order to handle such interstage floor shapes. This conclusion may also have important bearing on jet stagnation calculations when the jet is tilted with respect to the interstage floor axis.

IMPLICATIONS OF THE THEORETICAL-EXPERIMENTAL COMPARISONS

The important implication to design studies of the experimental and theoretical results is that in rocket staging problems the jet gas from the separation rocket may be confined to a thin, high density stream as it flows along the interstage floor. Thus, by supplying vents in the sides of the interstage at the level of the floor, much of the jet gas can be exhausted, and the interstage recirculation (and hence staging forces) can be greatly reduced. However, if vents are above the floor, even by a small amount, they may be much less effective, because the thin floor stream may be expected to require only a small height in which to complete its turn at the sides and begin re-accelerating toward the top of the interstage. For a design having simultaneous rocket ejection of two or more adjacent stages, strong flows exiting from any bottom vents would interact to produce a potentially strong flow up between the stages, which might produce high staging perturbations. This, of course, is the case for the Polaris A3 (Reference 1). Under these circumstances it might be better to avoid bottom venting entirely.

CONCLUSIONS

1. A ten week test program including 259 successful runs was conducted at the LMSC Tenney Altitude Facility. High pressure nitrogen was used to simulate flow from a rocket motor exhausting into the test cell at pressure altitudes which varied from 105,000 feet to 117,000 feet. Testing was completed on all the configurations planned with adequate pressure surveys, loads, and photographic data obtained to permit theoretical analysis.
2. The recirculation flow within an interstage during rocket powered stage separation appears to consist of a chain of supersonic accelerations and stagnations, each of which may be solved independent of the others. A method appears feasible for solving staging problems involving iteration on interstage cavity pressure, with calculation of the chain of stagnations around the interstage for each iteration.
3. The first stagnation of the separation rocket jet on the interstage floor appears to follow the laws of conservation of mass, axial momentum and radial momentum, as applied to the entire stagnation layer. A method for calculating this process with these equations appears feasible providing:
  - a. The correct position of the jet boundary is known;
  - b. The mass and momentum in the jet is properly apportioned between the isentropic core and the boundary strip;
  - c. The influence of the jet boundary in restricting the flow across the exit of the stagnation layer is properly considered.
4. In recirculation cases, the gas flow across the interstage floor appears confined to a thin layer due to the action of the jet boundary on the first stagnation flow field. This would be expected to render interstage vents at the level of the floor very effective in reducing recirculation forces. Likewise, for a cluster

of separating stages, sealing each interstage at the level of the floor would appear to be very effective in preventing recirculation in the center of the cluster.

REFERENCES

- (a) IMSC 804765, "Polaris B3 First Separation Analysis and Test Report", R. H. Brown, December 1964, Confidential
- (b) NASA TMX-870, "Interstage Pressures and Forces During High-Altitude Stage Separation with Operating Upper-Stage Engine", G. A. Mitchell and R. W. Cubbison, July 1963, Confidential
- (c) IMSC A188652, "Jet Wake Effects During Landing and Take-Off of a Lunar Excursion Module (LEM)", V. V. Baicher, R. R. Mikatarian and J. Huizinga, September 1962.
- (d) IMSC 919901, "PMS Jet Wake Study Program VN-10", R. J. Prozan, October 1961.
- (e) IDC 53-42-129, "Jet Impingement Program - Second Revision", V. V. Baicher, February 1964.
- (f) DP/M-500, "Method and Revised Equations to Obtain the Translational Forces Acting During First Separation", G. D. Reny, July 1960, Confidential
- (g) IMSC B028205, "Preliminary Analysis of the A3 Re-entry System Separation Test (P-32)", N. G. Tosch, April 1962 - SECRET
- (h) IDC, "Preliminary Gasdynamic Force-Distance Curves for A3 Re-entry System Separation", R. B. Stokes from N. G. Tosch, 12 December 1962
- (i) IMSC 803946, "Final Report on the Polaris A3 Re-entry System Separation Test (P-49)", N. G. Tosch, et. al, February 1964, Confidential
- (j) CC/81-30/247, "Summary Report - Vane Motion Studies DT 888 and DT 890", L. A. Burdick, October 1964
- (k) NASA TND-1095, "Interaction of Highly Under-Expanded Jets with Simulated Lunar Surfaces", L. E. Stitt, December 1961
- (l) IDC 55-12-32, "Gas Dynamic Interactions Independent Development Program - First Quarterly Review", V. V. Baicher, J. Huizinga, July 1964
- (m) "Flow Field of an Exhaust Plume Impinging on a Simulated Lunar Surface", D. W. Eastman and L. V. Radtke, AIAA Journal, I, #6, June 1963
- (n) AEDC-TR-59-11, "Spreading of Rocket Exhaust Jets at High Altitudes", E. K. Latvala, June 1959
- (o) "Rocket Exhaust Impingement on a Ground Surface", H. Yoshihara, J. Fluid Mech., 15 July 1962
- (p) NASA TN D-2327, "Comparison of Experimental Free-Jet Boundaries with Theoretical Results Obtained with the Method of Characteristics", A. R. Vick, E.H. Andrews, J. S. Dennard, C. E. Craidon, June 1964
- (q) "On the Structure of Jets from Highly Under-expanded Nozzles into Still Air", T. C. Adamson and J. A. Nickolls, J. Aerospace Sci., January 1959
- (r) "P-64 Test Computer Program", C. P. Ciallanza, O/59-32, November 1964

la,

TABLE I  
SONIC NOZZLE TEST SUMMARY

SEPARATION DISTANCE (exit radii)	10.9		16.3	19.0	217				32.6				38.0				42.4	43.5			
	N/A*	0			10.9	N/A	X	0	10.9	16.3	217	N/A	0	10.9	16.3	217		N/A	0	10.9	16.3
h - Fence Height (exit radii)																					
Flat Plate	X			X	X	X	X									X					
Flat Plate w/Nozzle Plate	X				X	X	X									X					
Flat Plate w/Fence		X	X														X	X	X	X	
Flat Plate w/Fence & Nozzle Plate																					
R/B Flare Simulation																X					
Flat Plate w/Nozzle Tilted 4.7°	X															X					
Flat Plate w/Nozzle Tilted 9.8°	X																				
Cone w/Altitude 21.7 radii																					

\*Not Applicable



TABLE II  
SUPERSONIC NOZZLE TEST SUMMARY

SEPARATION DISTANCE (exit radii)	4.5	6.8	8.0	9.1	10.2	11.3	12.5	13.3	13.6	14.8	15.9	18.1
h - Fence Height (exit radii)	N/A*	2.3 4.5	N/A 4.5	N/A 0 2.3 4.5	N/A 0 2.3 4.5	0 N/A	0 N/A	0 N/A	0 N/A	0 N/A	0 N/A	0 N/A
Flat Plate	X	X	X	X	X	X	X	X	X	X	X	X
Flat Plate w/Nozzle Plate	X	X	X	X	X	X	X	X	X	X	X	X
Flat Plate w/Fence	X	X	X	X	X	X	X	X	X	X	X	X
Flat Plate w/Fence & Nozzle plate	X	X	X	X	X	X	X	X	X	X	X	X
Flat Plate w/Nozzle Plate & Nozzle Tilted 10°												
Flat Plate w/Nozzle Plate, Fence & Nozzle Tilted 10°												

\*Not Applicable

TABLE III

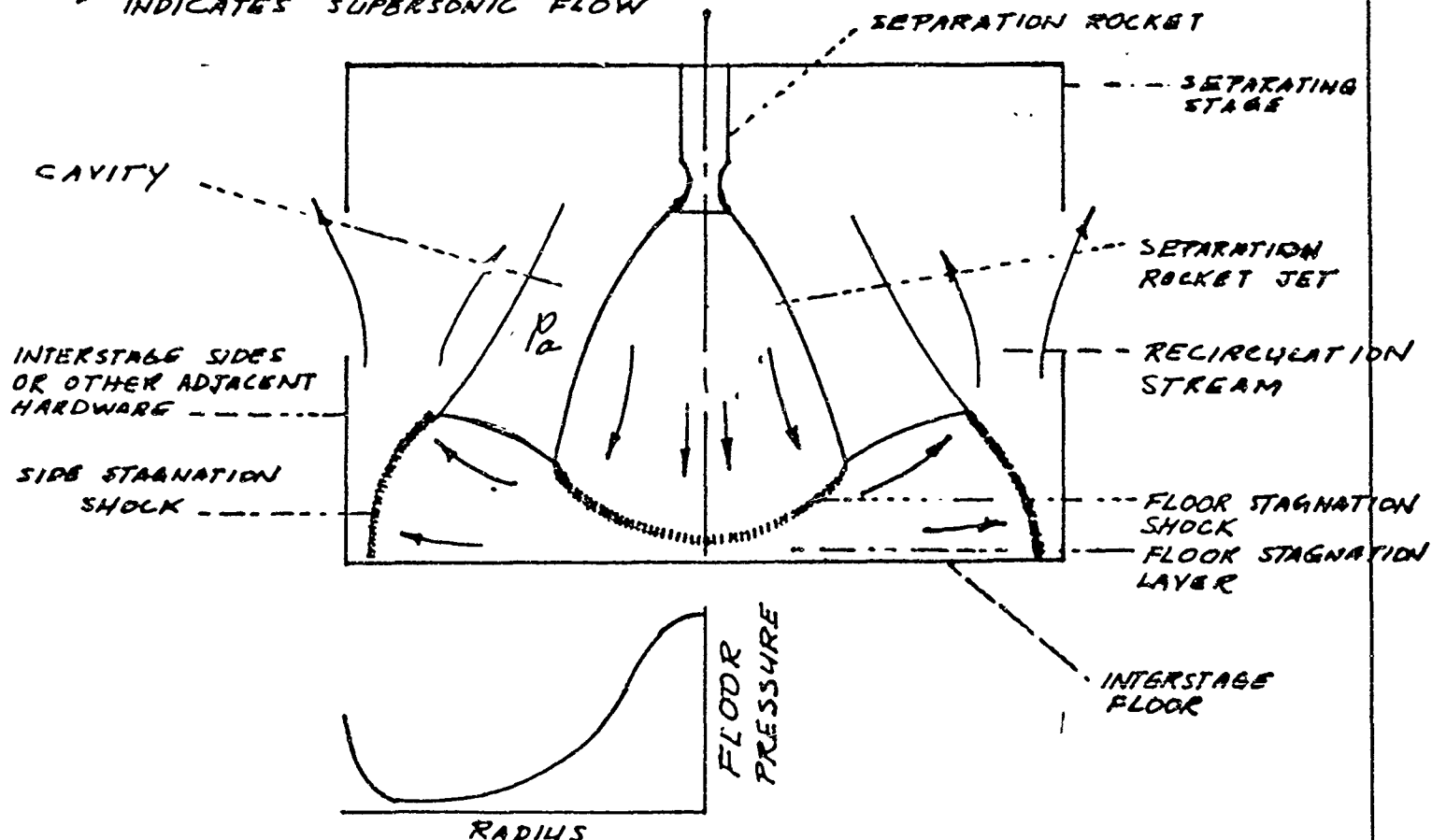
## ADJACENT JET SIMULATING FENCE - SONIC NOZZLE

SEPARATION DISTANCE (exit radii)	272	299	326	353	380	435	462	489
f - AJSF Separation Distance (exit radii)	54.3 65.2	54.3 65.2 76.1	54.3 65.2 76.1	46.2 54.3 65.2	46.2 54.3 65.2 76.1	46.2 54.3 65.2	46.2 54.3 65.2	46.2 54.3 65.2
180° Fence      h = 2.7		X			X	X		X
180° Fence      h = 5.4			X		X	X		X
180° Fence      h = 10.9						X		
120° Fence      h = 2.7	X	X	X		X	X	X	
120° Fence      h = 5.4				X	X	X	X	
60° Fence      h = 2.7			X			X		
60° Fence      h = 5.4		X	X		X	X		

Prepared	NAME	DATE	LOCKHEED MISSILES & SPACE COMPANY A GROUP DIVISION OF LOCKHEED AIRCRAFT CORPORATION	Page	TEMP	PERM
Checked			TITLE <b>NATURE OF RECIRCULATION</b>	Model		
Approved				Report No		

### a. RECIRCULATION FROM ADJACENT HARDWARE

→ INDICATES SUPERSONIC FLOW



### b. RECIRCULATION FROM ADJACENT FLOW

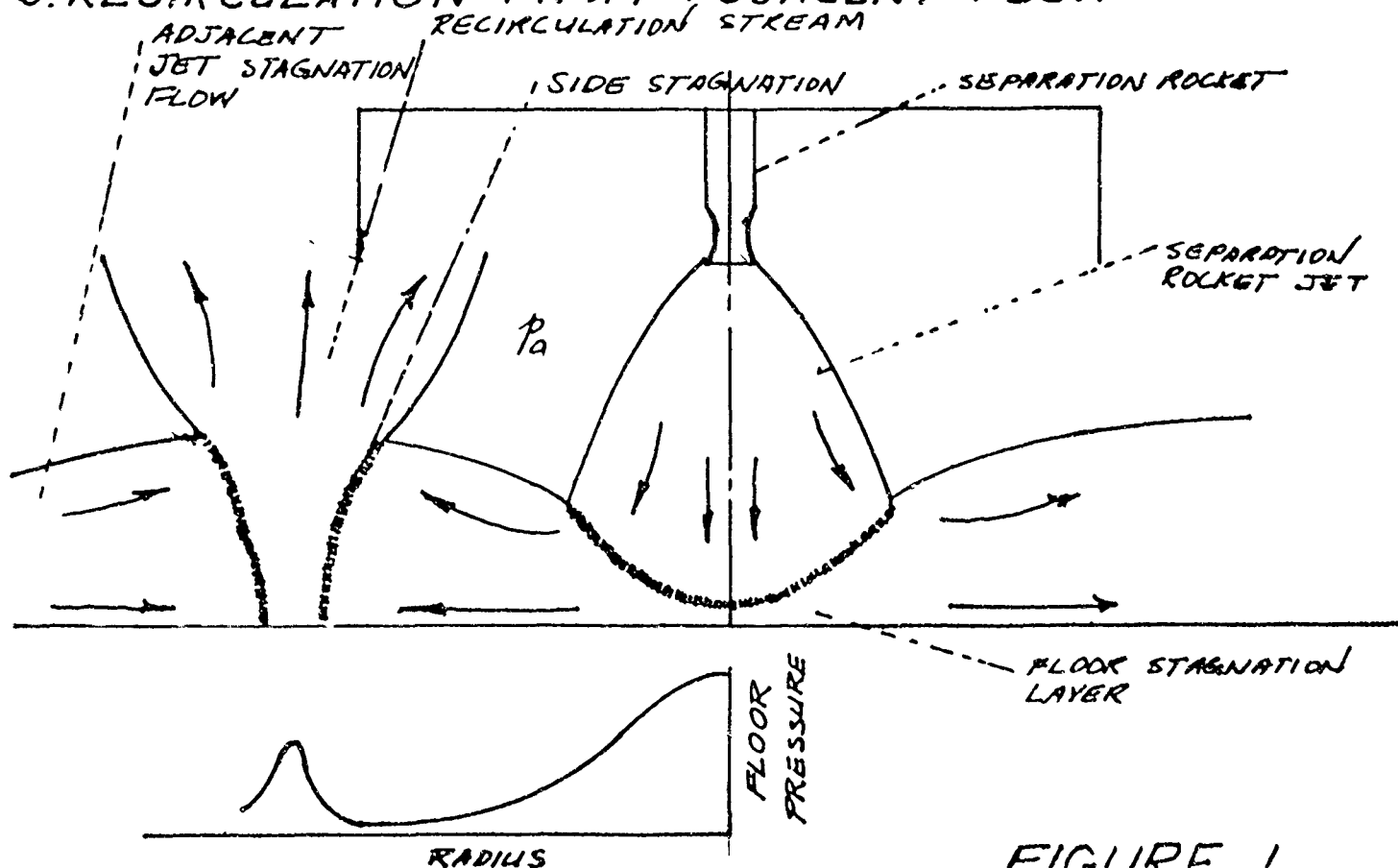


FIGURE 1

Prepared	NAME	DATE	LOCKHEED MISSILES & SPACE COMPANY A DIVISION OF LOCKHEED AIRCRAFT CORPORATION	Page	TEMP	PERM 34
Checked			TITLE <i>SEQUENCE OF TEST AND ANALYSIS CONFIGURATIONS</i>	Model		
Approved				Report No.		

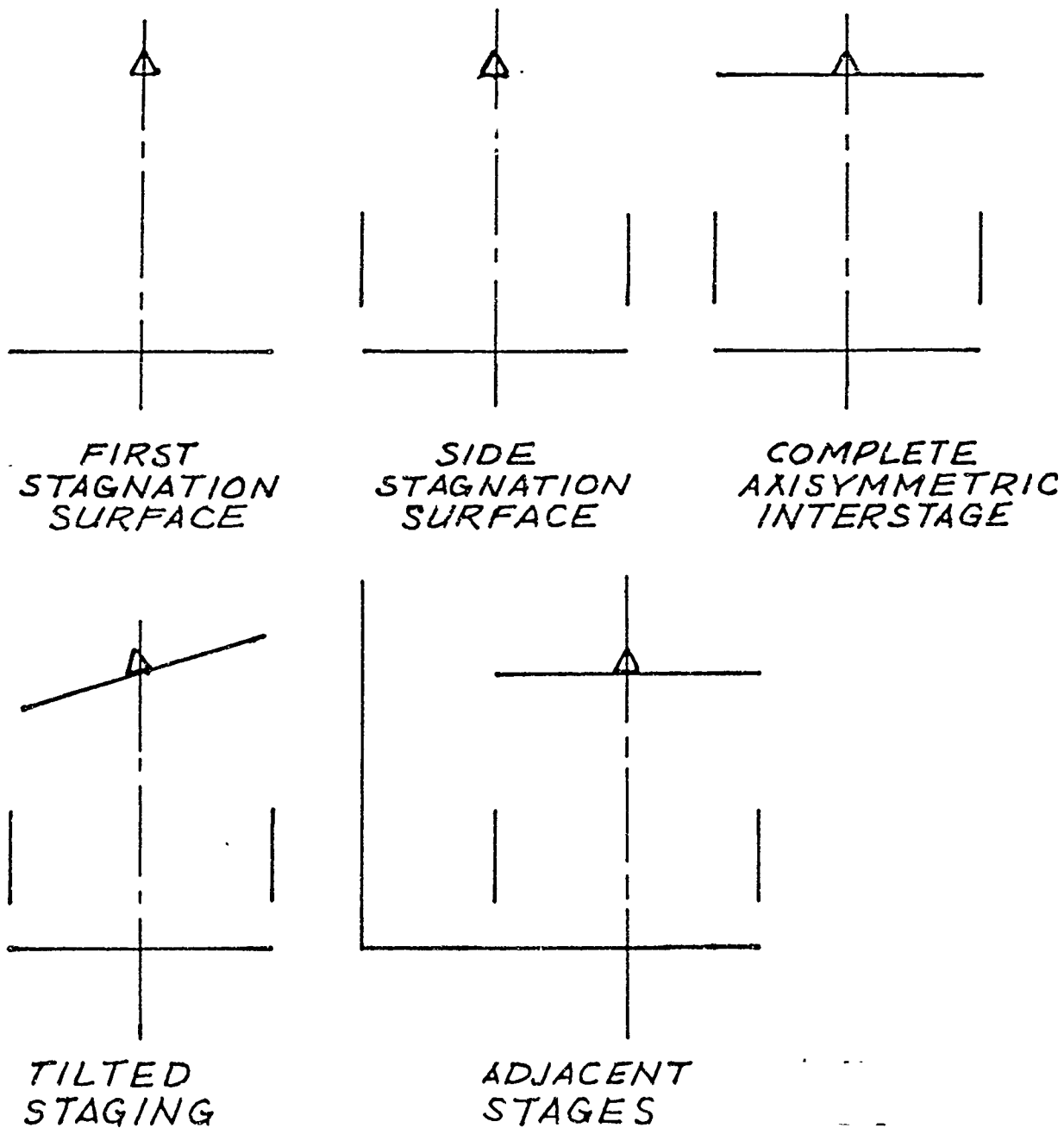
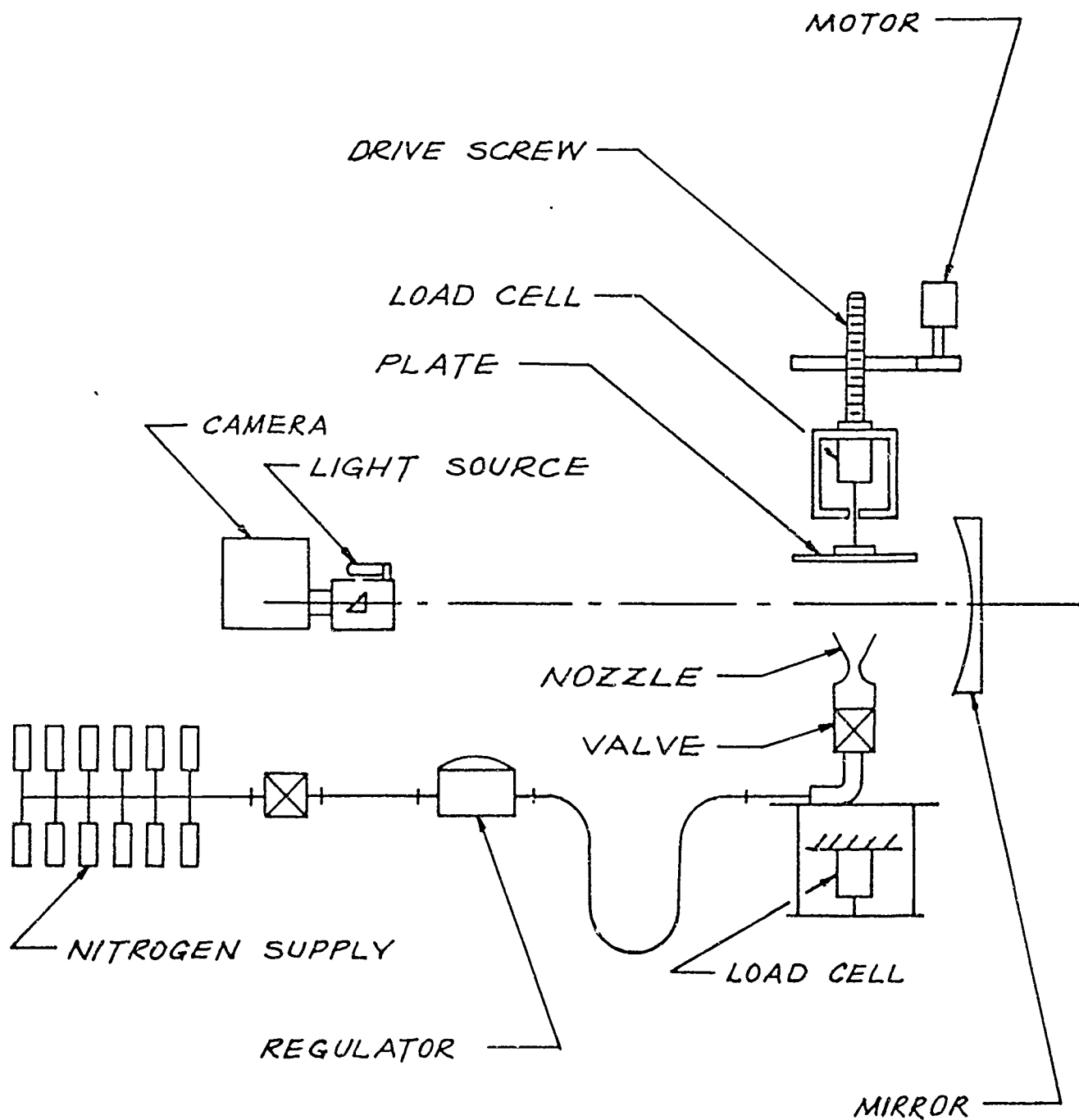


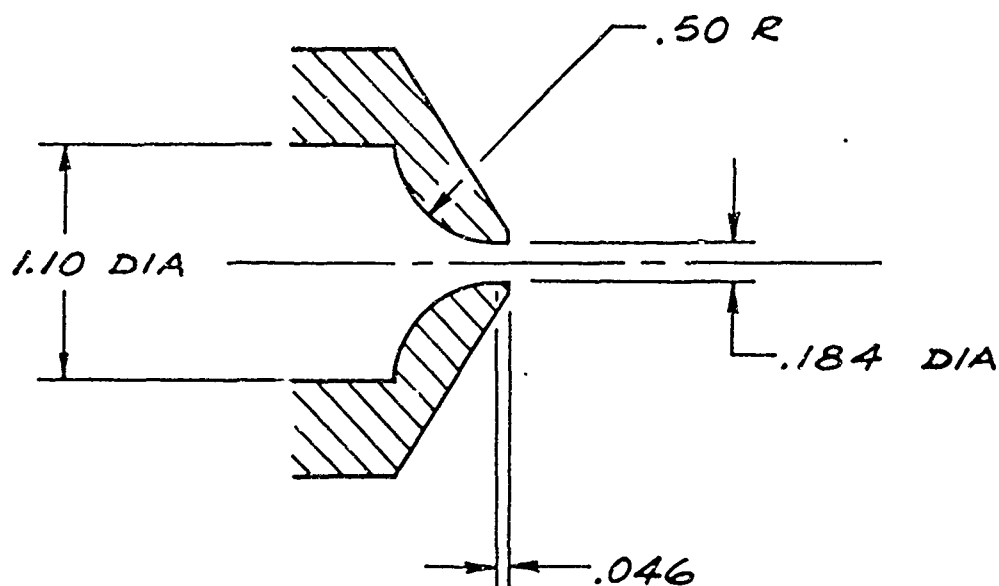
FIGURE 2

Prepared	NAME	DATE	LOCKHEED MISSILES & SPACE COMPANY A GROUP DIVISION OF LOCKHEED AIRCRAFT CORPORATION	Page	TEMP	PERM 35
Checked			TITLE <b>TEST SETUP</b>	Model		
Approved			<b>SCHEMATIC</b>	Report No		

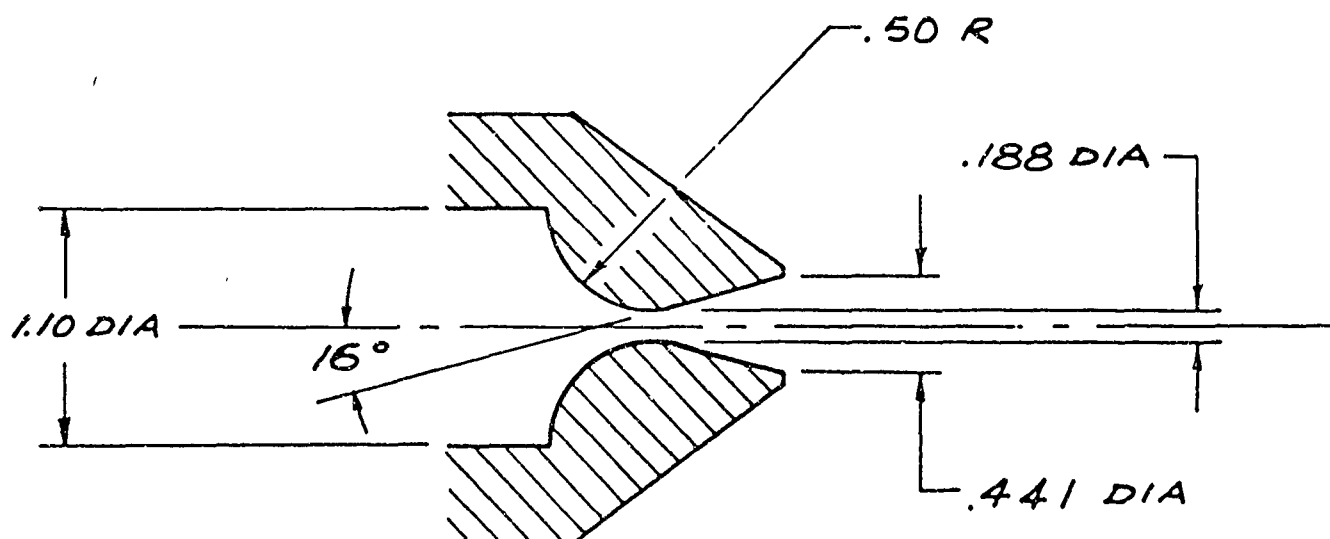


**FIGURE 3**

Prepared	NAME	DATE	LOCKHEED MISSILES & SPACE COMPANY A GROUP DIVISION OF LOCKHEED AIRCRAFT CORPORATION	Page	TEMP	PERM
Checked			TITLE <b>NOZZLE DETAILS</b>	Model		
Approved				Report No		



SONIC NOZZLE

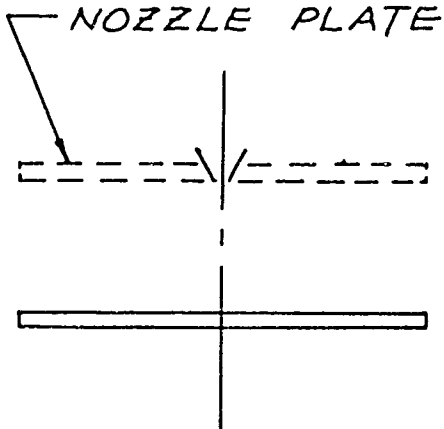


SUPERSONIC  
NOZZLE  
 $\epsilon = 5.5$

FIGURE 4

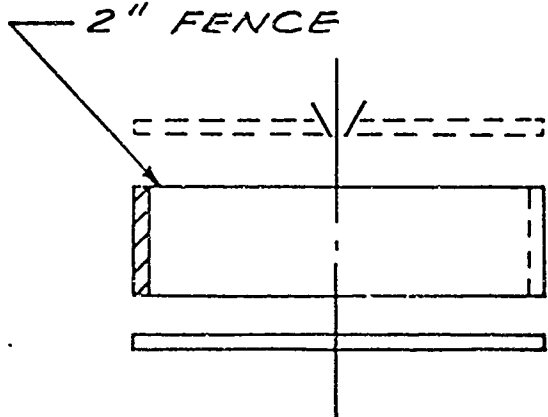
Prepared	NAME	DATE	LOCKHEED MISSILES & SPACE COMPANY A GROUP DIVISION OF LOCKHEED AIRCRAFT CORPORATION	Page	TEMP	PERM
Checked			TITLE <b>MODEL CONFIGURATIONS SCHEMATIC</b>	Model		37
Approved				Report No.		



NOZZLE PLATE

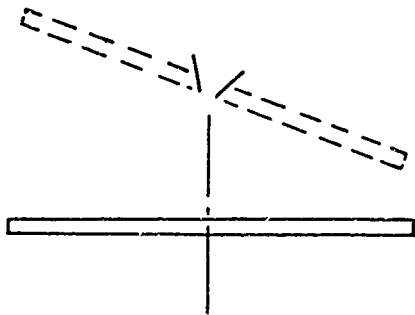
FLAT PLATE



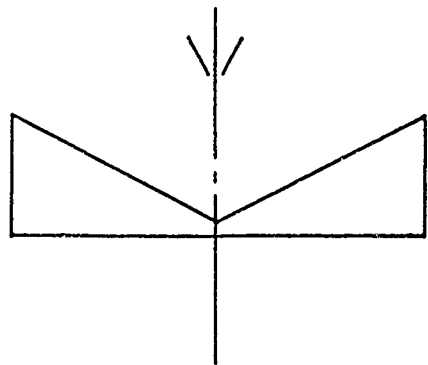
2" FENCE

VENTED CONTAINER

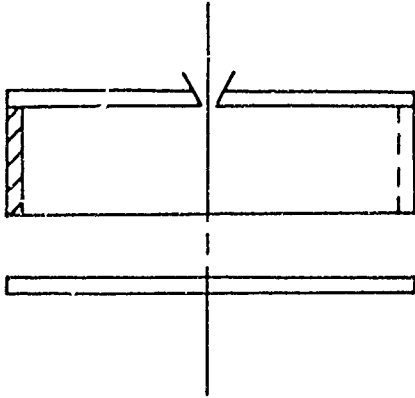


FLAT PLATE WITH  
TILTED NOZZLE

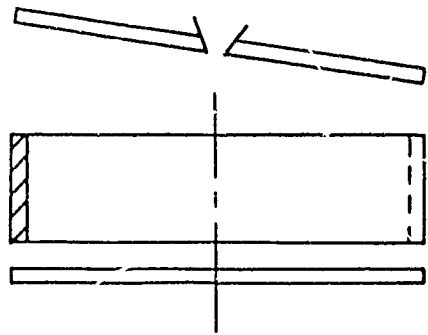


2" CONE



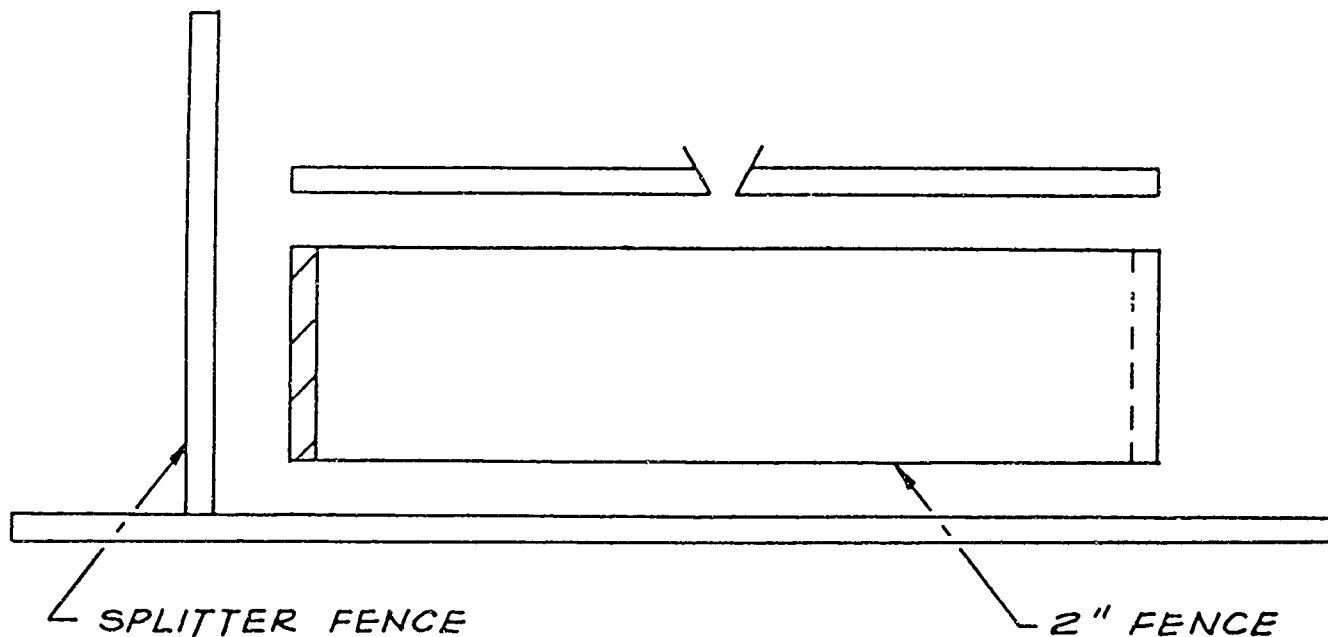
R/B FLARE



VENTED CONTAINER,  
TILTED NOZZLE  
WITH NOZZLE PLATE

FIGURE 5

Prepared	NAME	DATE	LOCKHEED MISSILES & SPACE COMPANY A GROUP DIVISION OF LOCKHEED AIRCRAFT CORPORATION	Page	TEMP	PERM
Checked			TITLE	MODEL		
Approved			CONFIGURATIONS			Model
			SCHEMATIC			Report No.



ADJACENT JET  
SIMULATING FENCES

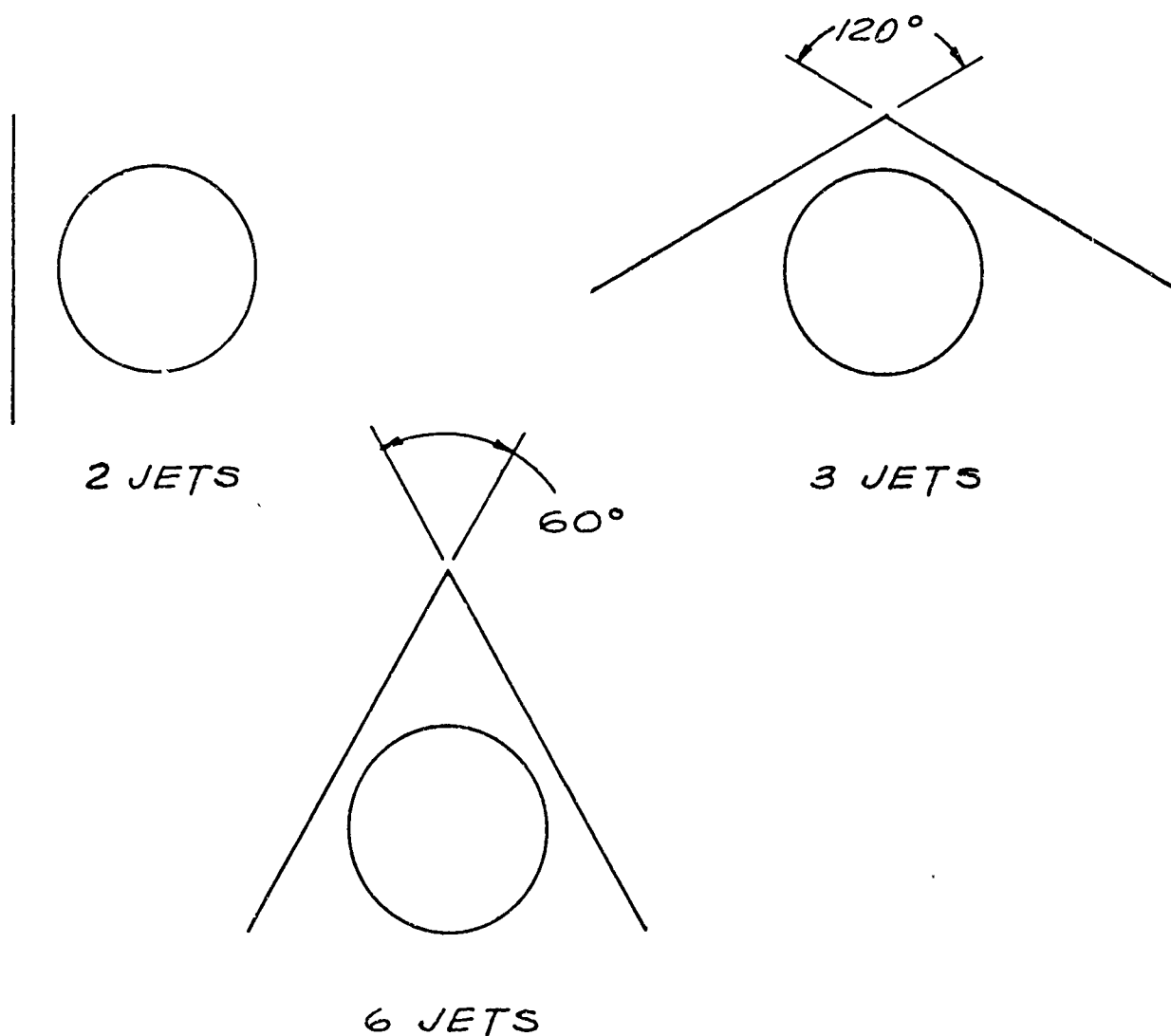


FIGURE 5 (CONT.)



Prepared	NAME	DATE	LOCKHEED MISSILES & SPACE COMPANY A GEORGETOWN AIRCRAFT CORPORATION	Page	TEMP	PERM
Checked			TITLE <i>NOMENCLATURE</i>	Model		39
Approved				Report No		

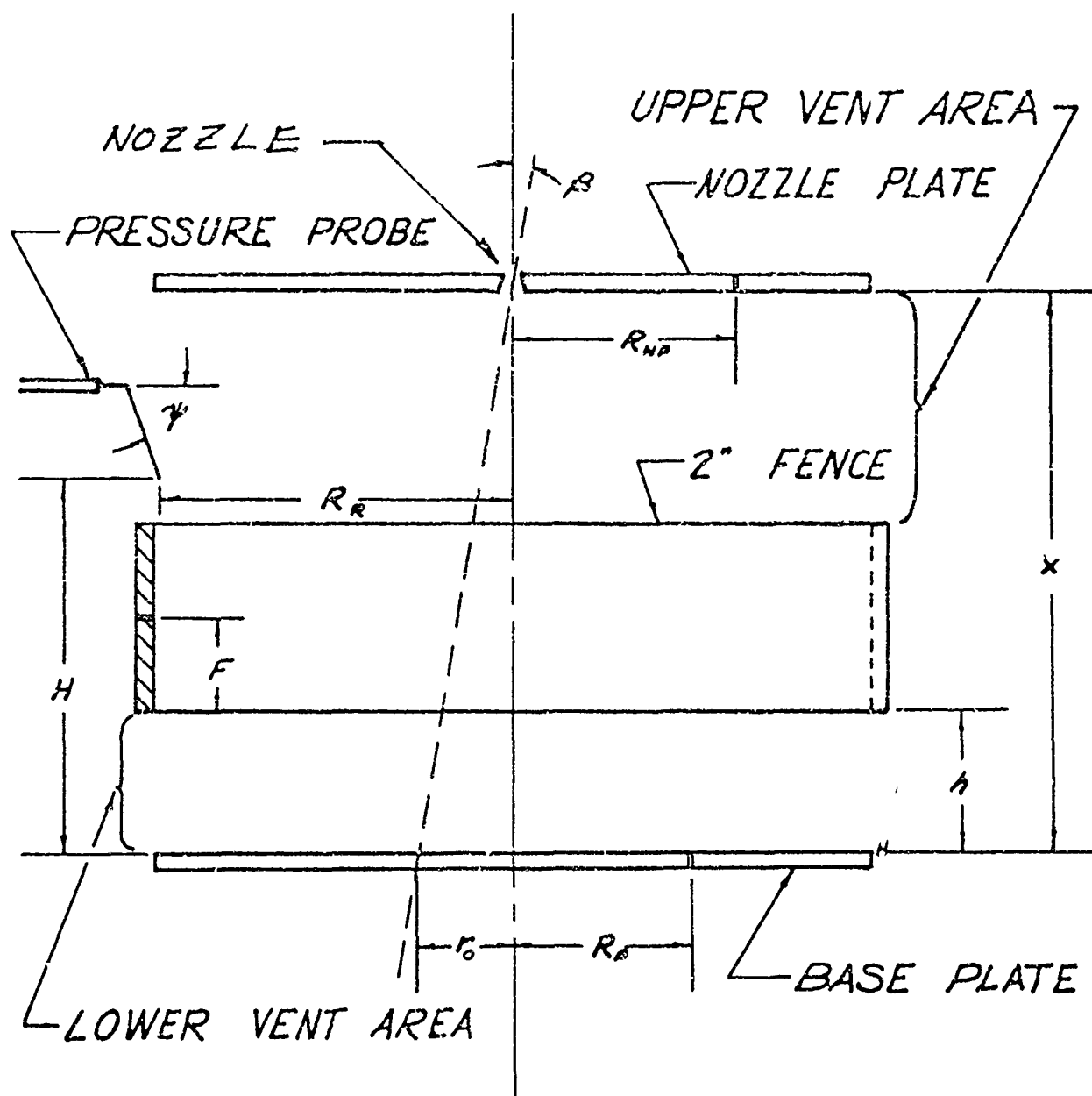


FIGURE 6

Prepared	NAME	DATE	LOCKHEED MISSILES & SPACE COMPANY A GEORGETOWN UNIVERSITY RESEARCH CORPORATION	Page	TEMP	PERM
Checked			TITLE	Model		
Approved			ADJACENT JET SIMULATING CONFIGURATION	Report No		40

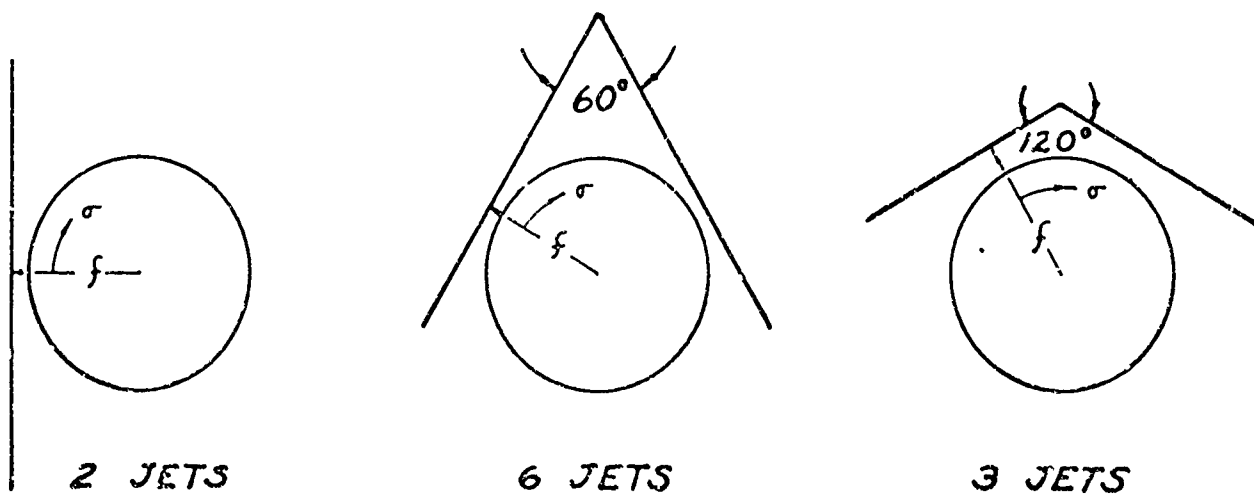
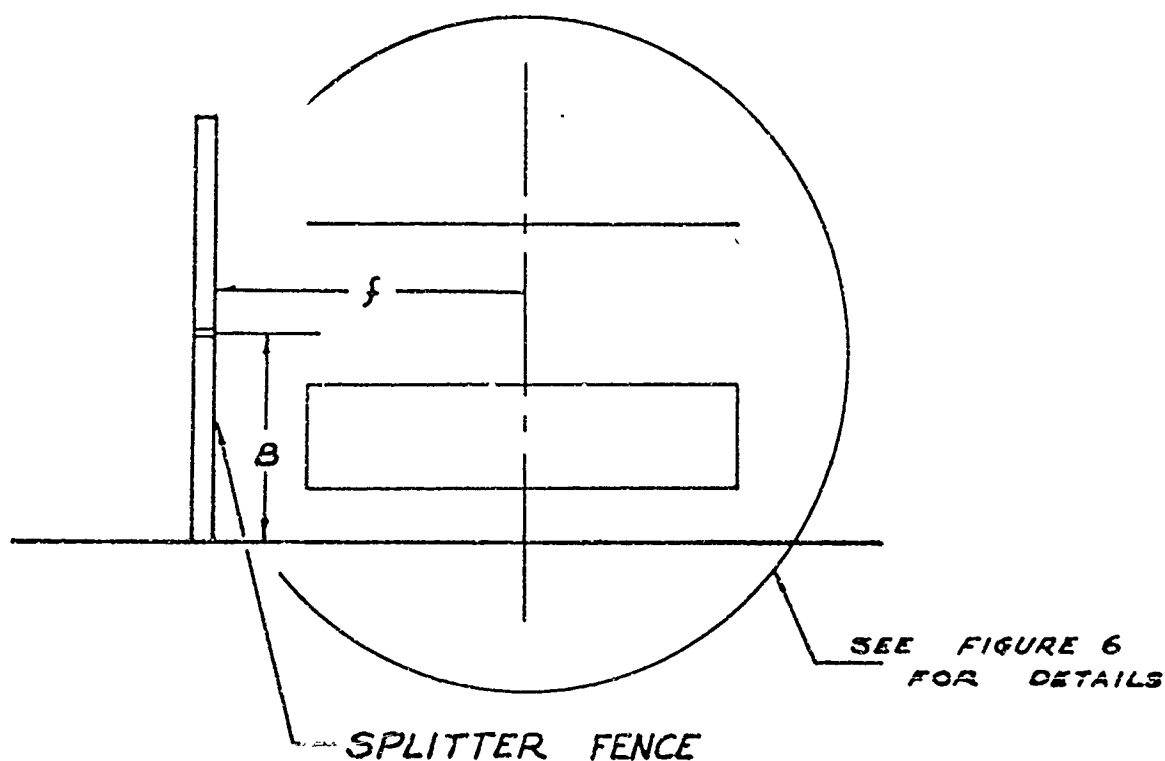


FIGURE 7



Prepared	NAME	DATE	LOCKHEED MISSILES & SPACE COMPANY A GEORGE EASTMAN COMPANY OF LOCKHEED AIRCRAFT CORPORATION	Page	TEMP	PERM
Checked			TITLE	Model		
Approved			COMPARISON OF THEORY AND EXPERIMENT	Report No		42

### CASE 1

SONIC TEST NOZZLE AT 10.9 in, NORMAL TO A  
FLAT PLATE.  $P_{Tn}/P_0 = 12,000$ .  $P_{Tn} = 1000$

———— EXPERIMENT  
 - - - - - THEORY OF APPENDIX I  
 ..... THEORY WITH ADJUSTED BOUNDARY  
 ○ ○ METHOD OF CHARACTERISTICS

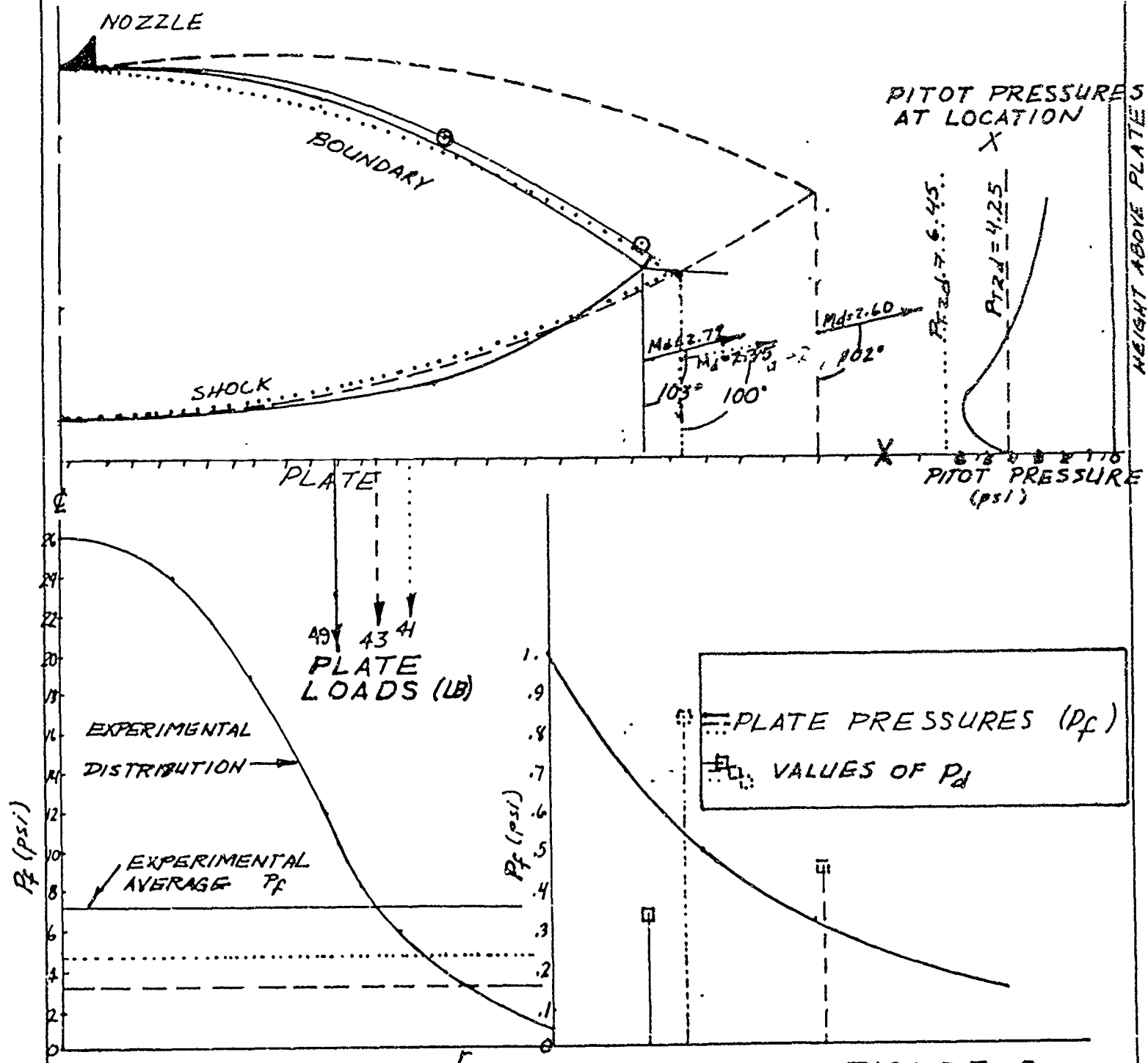


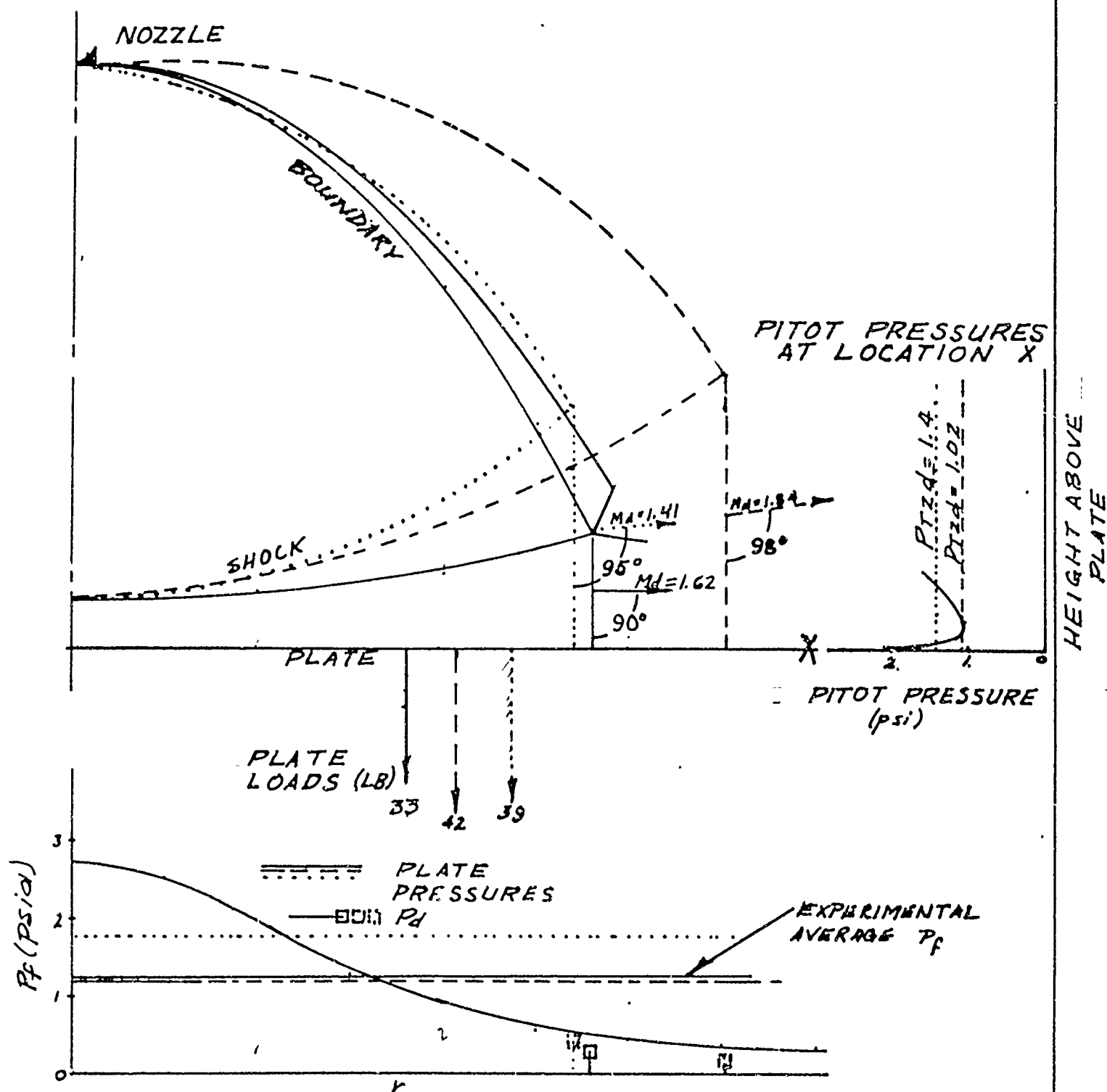
FIGURE 9

Prepared	NAME	DATE	LOCKHEED MISSILES & SPACE COMPANY A DIVISION OF LOCKHEED AIRCRAFT CORPORATION	Page	TEMP	PERM
Checked			TITLE COMPARISON OF THEORY AND EXPERIMENT	Model		
Approved				Report No		43

## CASE 2

SONIC TEST NOZZLE AT 32.5 in NORMAL TO A  
FLAT PLATE.  $P_{Tn}/P_s = 12000$   $P_{Tn} = 1000$

———— EXPERIMENT  
 ----- THEORY OF APPENDIX I  
 ..... THEORY WITH ADJUSTED BOUNDARY



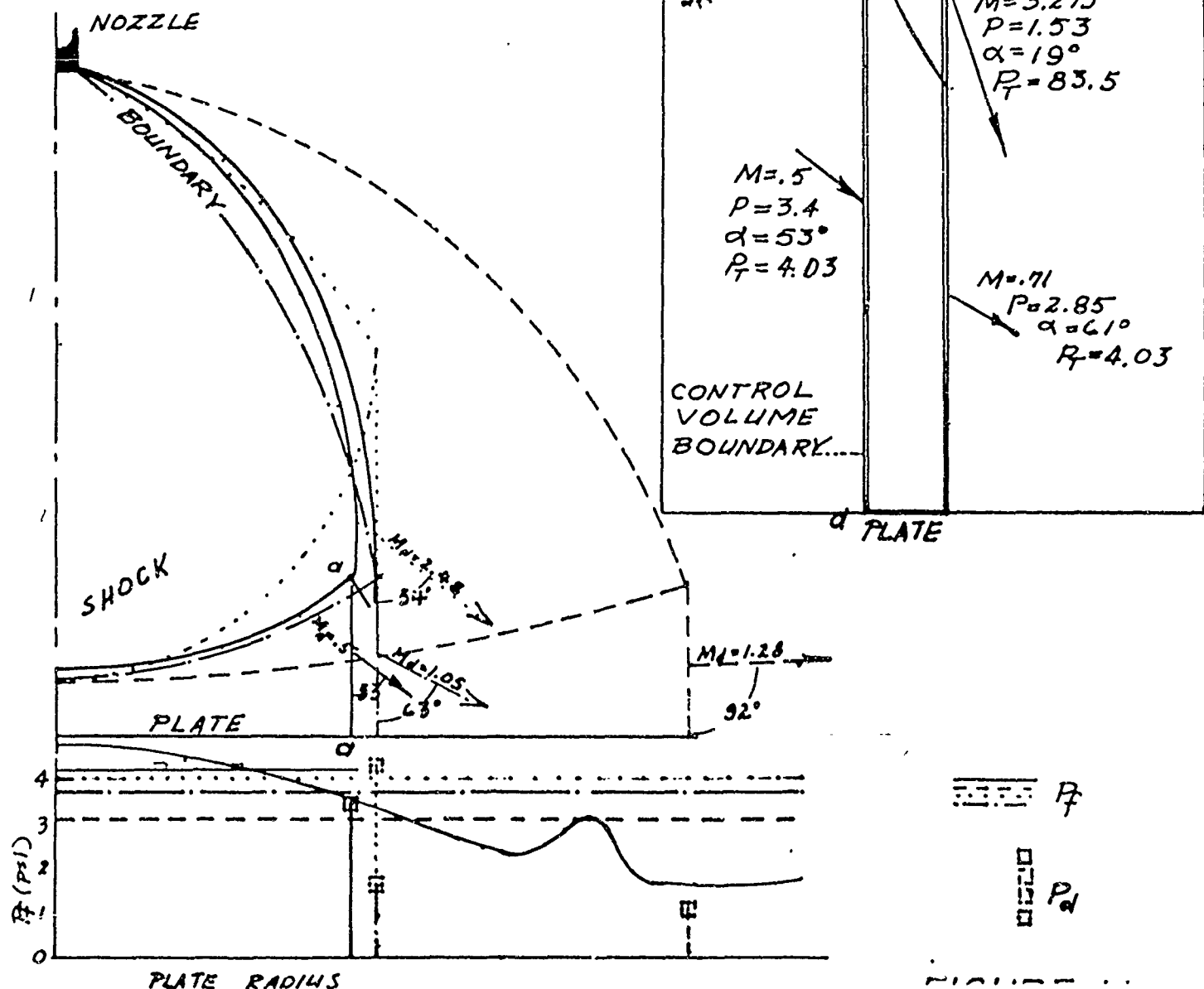
Prepared	NAME	DATE	LOCKHEED MISSILES & SPACE COMPANY A GROUP DIVISION OF LOCKHEED AIRCRAFT CORPORATION	Page	TEMP	PERM 44
Checked			TITLE COMPARISON OF THEORY AND EXPERIMENT	Model		
Approved				Report No		

### CASE 3

SONIC TEST NOZZLE AT 32.5  $r_n$  NORMAL TO A  
FLAT PLATE.  $P_{Tn}/P_a = 1130$ .  $P_{Tn} = 1500$ .

- EXPERIMENT  
 - - - - - THEORY OF APPENDIX I  
 ..... THEORY WITH ADJUSTED BOUNDARY  
 - · - · - THEORY WITH ADJUSTED BOUNDARY,  
 JET MASS, AND JET MOMENTUM

INTERACTION BETWEEN  
BOUNDARY AND STAGNATION  
LAYER STREAMS AT  $\alpha = 0$



Prepared	NAME	DATE	LOCKHEED MISSILES & SPACE COMPANY A GROUP DIVISION OF LOCKHEED AIRCRAFT CORPORATION	Page	TEMP	PERM 45
Checked			TITLE	Model		
Approved				Report No.		

# COMPARISON OF JET BOUNDARY APPROXIMATIONS

$$M_n = 1.0 \quad \alpha_n = 0^\circ \quad R_n/P_2 = 1314$$

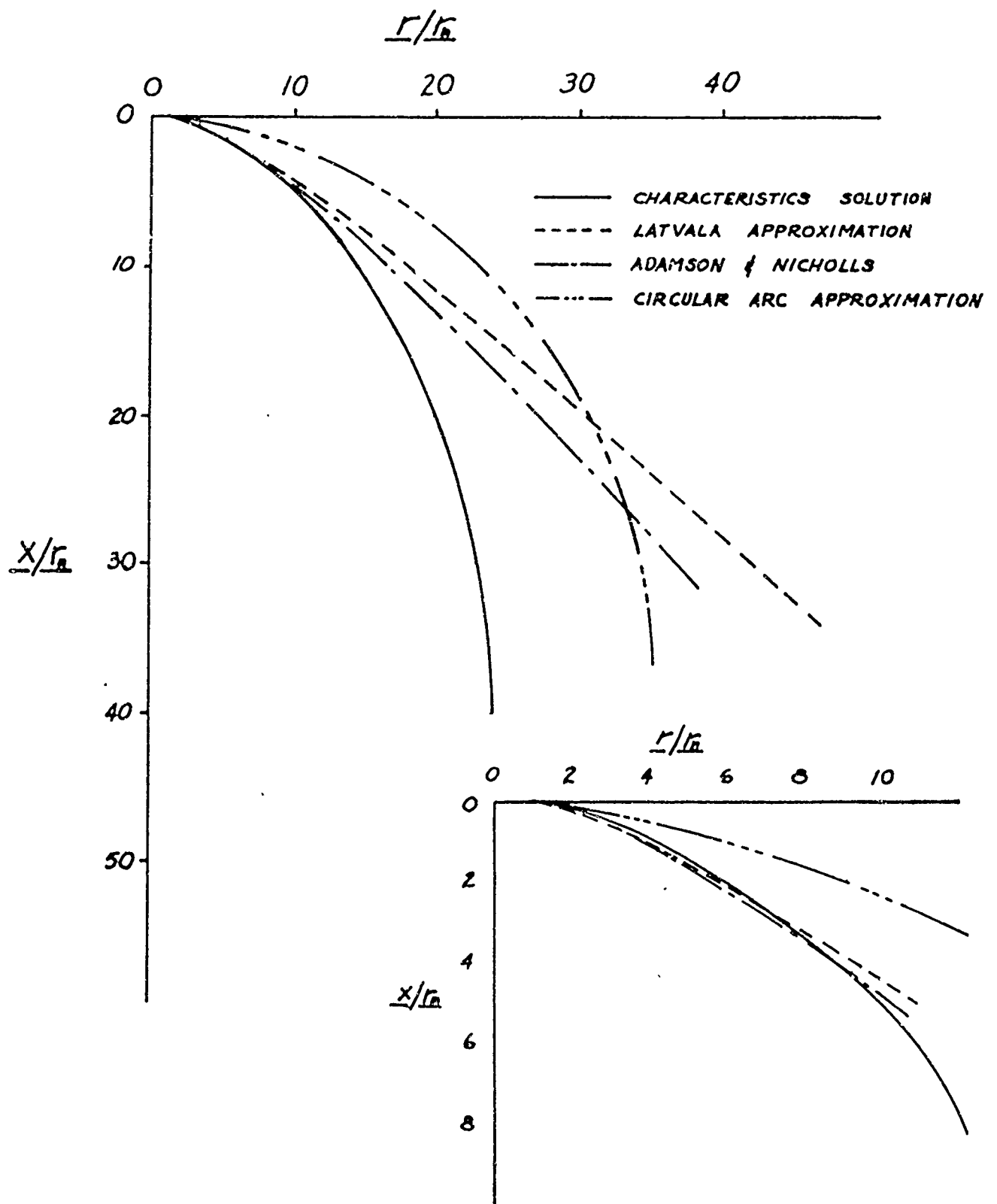
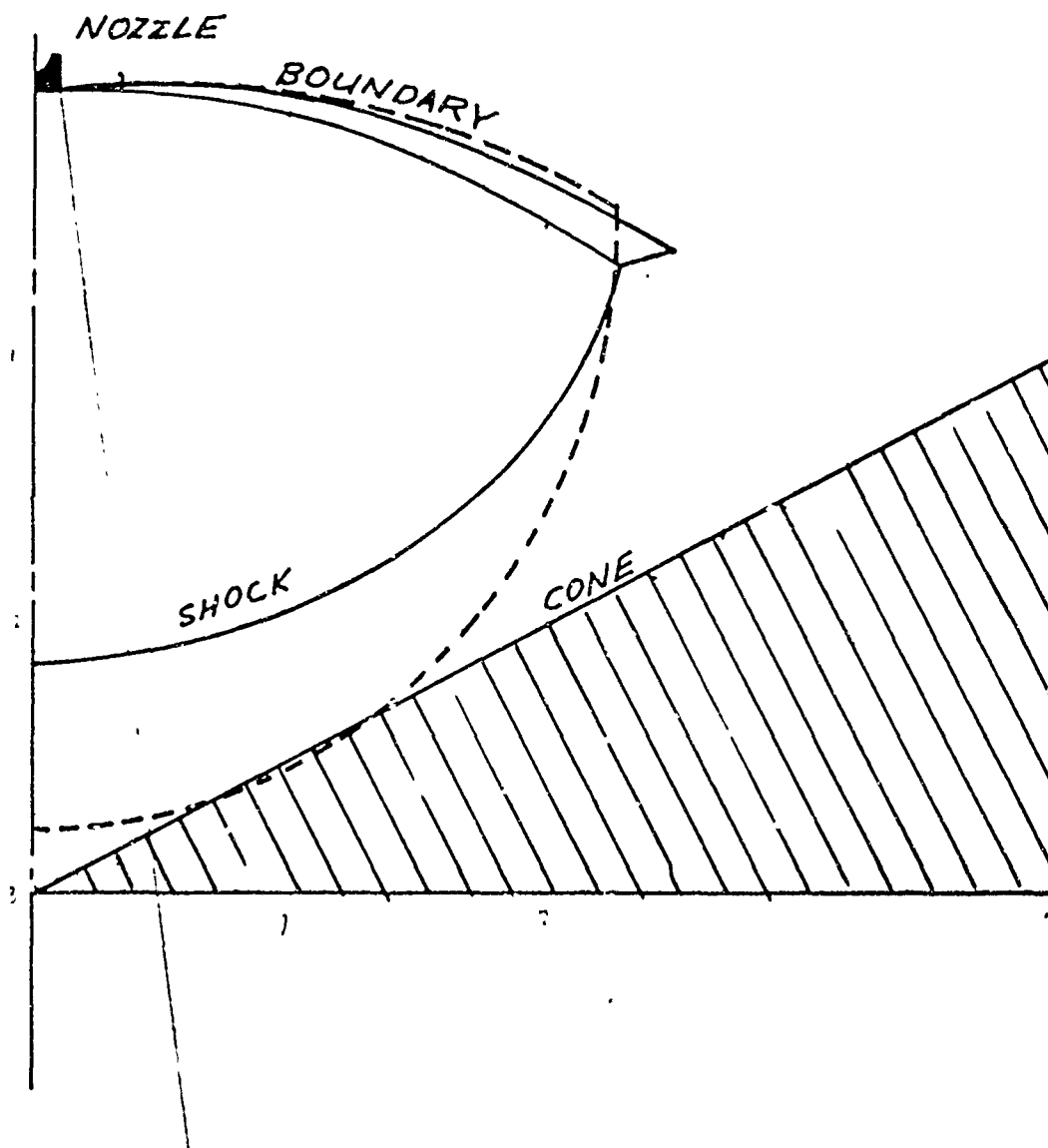


FIGURE 12

Prepared	NAME	DATE	LOCKHEED MISSILES & SPACE COMPANY A GROUP DIVISION OF LOCKHEED AIRCRAFT CORPORATION	Page	TEMP	PERM 46
Checked			TITLE COMPARISON OF THEORY AND EXPERIMENT	Model		
Approved				Report No.		

CASE 4  
SONIC TEST NOZZLE AT 32.5  $r_n$  FROM THE  
CENTER OF AN INVERTED COAXIAL CONE

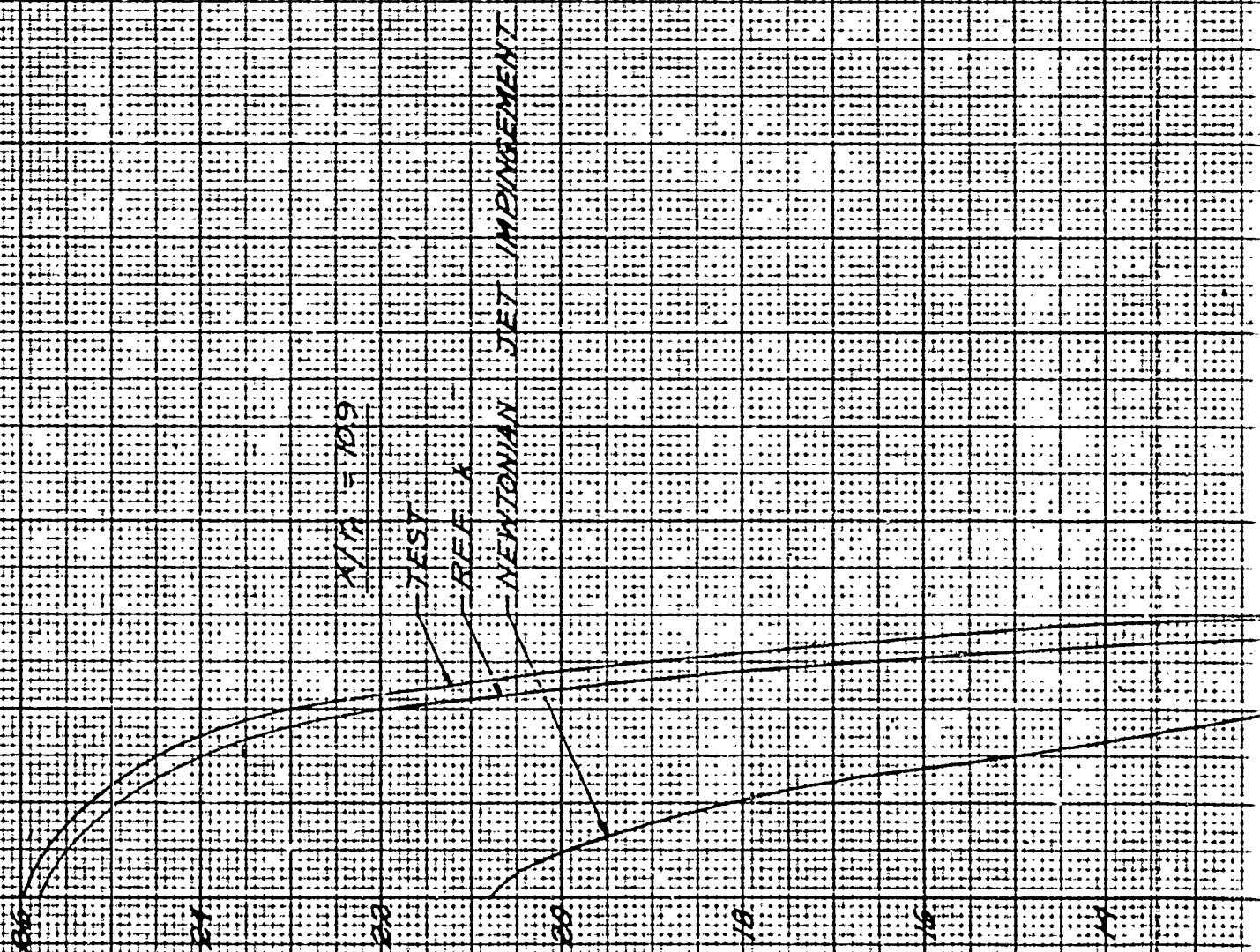
—— EXPERIMENT  
----- THEORY OF APPENDIX I.



NOTE:  
MATHEMATICAL DIFFICULTIES  
PREVENTED COMPLETION OF  
THE THEORETICAL SOLUTION.



# COMPARISON OF RES 501°C NOZZLE NORMAL IMPINGEMENT PLATE PRESSURE DISTRIBUTION



A

RESULTS  
MENT ON FLAT PLATE  
DISTRIBUTION

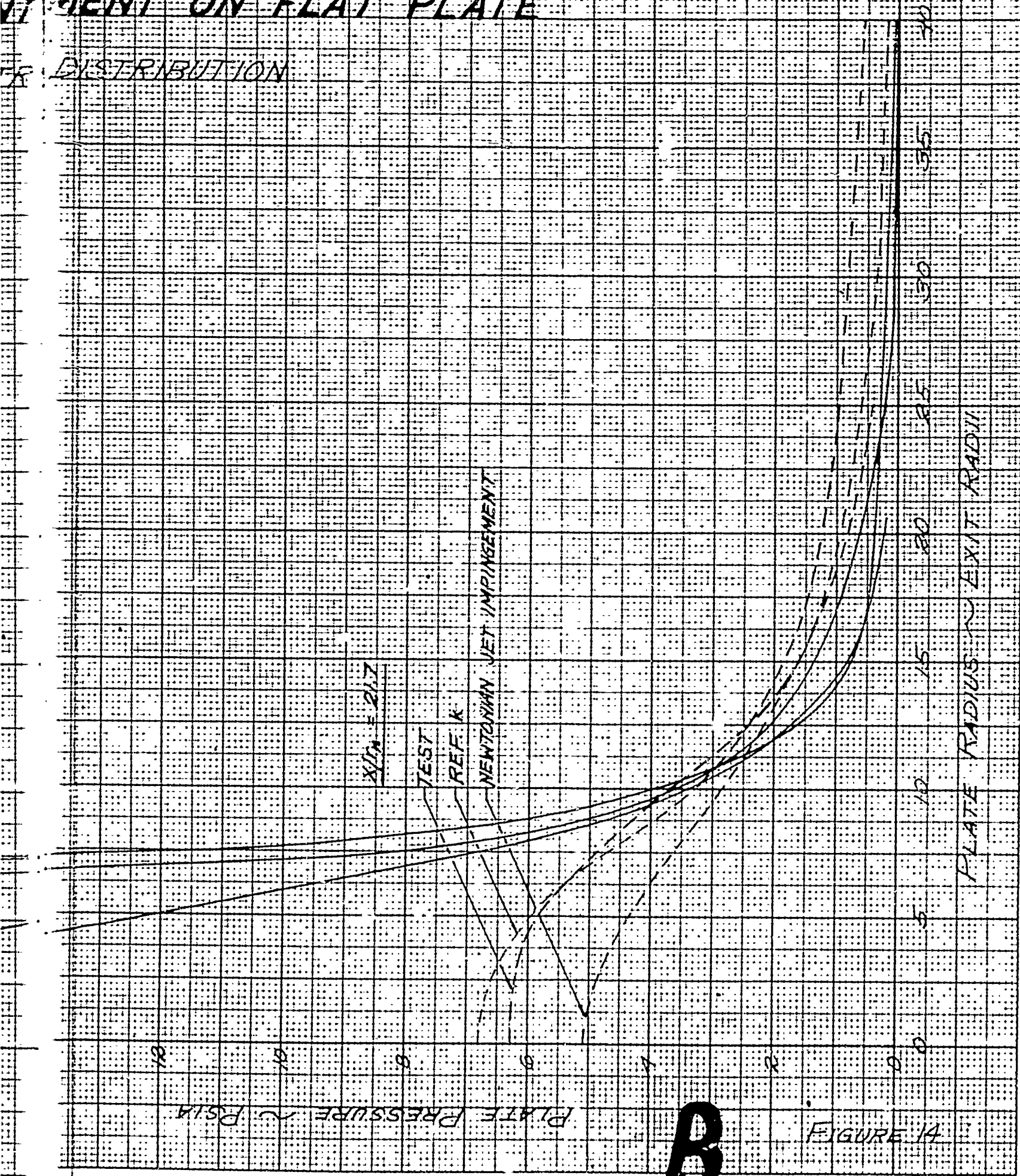


FIGURE 14

## APPENDIX I

### CONTROL VOLUME METHOD FOR AN AXISYMMETRIC FIRST STAGNATION

### Basic Assumptions

As shown in Figure (8), an axisymmetric free jet is assumed to expand from the separating body nozzle to the interstage pressure environment, and stagnate against an axisymmetric interstage floor having the same axis as the nozzle and jet. The gas is assumed perfect, with ratio of specific heats ( $\gamma$ ) constant at the nozzle chamber value. The entire flow field is assumed steady. The jet expansion and stagnation processes are assumed adiabatic, with the flow in the jet isentropic except for a small region near the boundary. The flow properties in the free jet can thus be obtained with the method of characteristics (Reference d). The flow in the layer (V) is also assumed isentropic, so that all entropy changes in the field occur at the shock, s.

### Basic Equations

The basic equations used are conservation of the mass, axial (x) momentum and radial (r) momentum of the gas within control volumes. These equations hold if the flow is steady, adiabatic, and perfect. Under these conditions the conservation of energy is not independent of conservation of mass and momentum. The mass and momentum equations are written for Volume V of Figure 8, with mass and axial momentum fluxes into V determined from the fluxes out of  $V_1$ .

Since the flow is assumed steady, conservation of mass in V and  $V_1$  takes the form:

$$(\text{mass flow into volume}) = (\text{mass flow out of volume})$$

For  $V_1$  (see list of symbols):

$$\dot{m}_{out} = \frac{\theta P_{Tn} r_*^2}{2 \left( \frac{\gamma+1}{2} \right)^{\frac{\gamma+1}{2(\gamma-1)}}}$$

For V,  $\dot{m}_{in} = \dot{m}_{out}$  out from  $V_1$ . Thus:

$$1. \quad \frac{P_{Tn} r_*^2}{2 \left( \frac{\gamma+1}{2} \right)^{\frac{\gamma+1}{2(\gamma-1)}}} = p_d r_d \Delta x_d \sin \alpha_d M_d \sqrt{1 + \frac{\gamma-1}{2} M_d^2}$$

where  $p_d$ ,  $\alpha_d$ , and  $M_d$  refer to average values across the stagnation layer at d

(as defined in the list of symbols), and  $\theta$  has been divided out.

Conservation of axial momentum in the volumes has the form:

$$\begin{aligned} & (\text{flux of x-momentum into volume}) + (\text{integral of all pressure} \\ & \text{forces on the volume in the positive x-direction}) - \\ & (\text{flux of x-momentum out of volume}) = 0 \end{aligned}$$

since the flow is steady and no external forces are applied except along the bounding surfaces of the volumes. for volume  $V_1$ :

$$\begin{aligned} & (\text{flux of x-momentum out of volume} + \text{pressure force on shock surface, } s, \\ & \text{in the negative x-direction}) = \end{aligned}$$

$$\frac{\theta (1 + \gamma M_n^2) P_{Tn} r_n^2}{2 \left(1 + \frac{\gamma-1}{2} M_n^2\right)^{\frac{\gamma}{\gamma-1}}} + \frac{\theta}{2} P_a (r_d^2 - r_n^2)$$

For volume  $V$ , the flux of x-momentum in over  $s$  + the pressure force in the positive x-direction on  $s$ , is equal to the left-hand side of the above equation.

Hence:

$$\begin{aligned} 2. \quad & \frac{(1 + \gamma M_n^2) P_{Tn} r_n^2}{\left(1 + \frac{\gamma-1}{2} M_n^2\right)^{\frac{\gamma}{\gamma-1}}} + P_a (r_d^2 - r_n^2) - 2 \int_0^{r_d} P_f(r) r dr \\ & - 2 \gamma P_d r_d \Delta x_d \sin \alpha_d \cos \alpha_d M_d^2 = 0 \end{aligned}$$

where  $\theta/2$  has been divided out. Here,  $\int_0^{r_d} P_f r dr$  is the pressure force exerted on  $V$  in the negative x-direction by the interstage floor.

Under the basic assumptions, conservation of radial momentum in volume  $V$  has the form:

$$\begin{aligned} & (\text{flux of r-momentum into } V \text{ across surface } s) \\ & + (\text{positive } r \text{ component of the pressure force acting on } s) \\ & + (\text{positive } r \text{ component of the pressure force on the sides, } m, \text{ of} \\ & V) + (\text{positive } r \text{ component of the pressure force exerted by the inter-} \\ & \text{stage floor, } f) - (\text{flux of r-momentum out of } V \text{ across } d) - (r \text{ component of} \\ & \text{pressure force acting on the exit, } d, \text{ of } V) = 0 \end{aligned}$$

Denoting the sum of the first two terms by  $T_{jr}$ , we have:

$$3. \quad T_{jr} + 2 \sin \frac{\Theta}{2} \int_0^{r_d} \int_{x_s}^{x_f} P_f(x, r) dx dr + \Theta \int_{x_{fc}}^{x_{fd}} P_f(r) r_f^f(x) dx - P_d r_d \Delta x_d \Theta (1 + \gamma M_d^2 \sin^2 \alpha_d) = 0$$

Equations 1, 2, and 3 are the basic equations used in the solution to the first stagnation problem. The desired answers are the flow properties and geometry ( $P_d, M_d, \alpha_d, r_d, \Delta x_d$ ) at the exit, d, of the stagnation layer, and the total load on the interstage floor under the layer ( $2\pi \int_0^{r_d} P_f(r) r dr$ ).

#### Assumptions

In addition to the desired flow properties ( $P_d, M_d, \alpha_d$ ), the geometry of the stagnation layer exit ( $r_d, \Delta x_d$ ), and the interstage floor pressure distribution ( $P_f(r)$ ), equations 1 - 3 contain the radial thrust of gas crossing s ( $T_{jr}$ ), the static pressure distribution in the layer ( $P_f(x, r)$ ), and the shock shape ( $x_s(r)$ ). There are thus 9 unknown quantities and functions to be determined with 3 equations. This requires assumptions permitting 6 of the unknown quantities to be calculated or related to other unknowns.

If the jet boundary shape is known,  $r_d$  is related to  $\Delta x_d$  by simple geometry involving the known interstage floor shape. In this method the jet boundary is assumed to be given by a Latvala circular arc (Reference n), as follows (see Figure 8 and list of symbols):

$$4. \quad \alpha_{bn} = \nu(M_b) - \nu(M_n) + \alpha_n$$

$$\text{where: } \nu(M) = \sqrt{\frac{\gamma+1}{\gamma-1}} \tan^{-1} \sqrt{\frac{\gamma-1}{\gamma+1} (M^2-1)} - \tan^{-1} \sqrt{M^2-1}$$

$$\text{and: } M_b = \sqrt{\frac{2}{\gamma-1} \left[ \left( \frac{P_{Tn}}{P_a} \right)^{\frac{\gamma-1}{\gamma}} - 1 \right]}$$

$$5. \quad P_b = r_n \left[ \frac{15.25}{M_n - .377} + 13.78 \right] \sqrt{\frac{(\gamma+1)(5+M_n^2)}{M_n^2}}$$

In order to relate the shock shape,  $x_s(r)$ , to  $\Delta x_d$  and  $r_d$ , it is necessary to know the point,  $x_{sc}$ , where the shock crosses the axis of symmetry, and also the shape function of the shock. In this method,  $\delta_s$  is assumed to be given by the Yoshihara analysis (Reference c):

$$6. \quad \delta_s = \frac{x_{sc}}{2} \left[ \frac{\gamma-1}{\gamma+1} + \frac{1}{M_{jc}^2(x_{sc})} \right]$$

$$x_{sc} = x_{fc} - \delta_s$$

where  $M_{jc}(x_{sc})$  is the Mach number in the free jet at the point where the shock crosses the axis, as given by the method-of-characteristics program of Reference d. Since  $M_j$  varies with  $x_{sc}$ , equations 6 must be solved iteratively.

The shape of the shock is assumed in this analysis to be a spherical cap, with center on the axis of symmetry. This assumption, together with the locations of two points on the shock ( $x_{sc}$ , and  $x_{sd}, r_d$ ), is sufficient to determine  $x_s(r)$ :

$$7. \quad \rho_s = \frac{(x_{sc} - x_{sd})^2 + r_d^2}{2(x_{sc} - x_{sd})}$$

$$\phi_s(r) = \sin^{-1} \frac{r}{\rho_s}$$

$$x_s(r) = \rho_s [\cos \phi_s(r) - 1] + x_{sc}$$

Where  $\phi_s$  is the angle between the normal to the shock at the point ( $x_s, r$ ), and the axis of symmetry.

With the shock shape known,  $T_{jr}$  may be determined, since the flow properties in the free jet are given by method-of-characteristics:

$$8. \quad T_{jr} = \rho_s^2 \theta \int_0^{\phi_{sd}} p_j [\gamma M_j^2 \cos(\alpha_j - \phi_s) \sin \phi_s \sin \alpha_j + \sin^2 \phi_s] d\phi_s$$

here,  $p_j$ ,  $\alpha_j$ , and  $M_j$  are the flow properties in the free jet at the point:

$$x = x_{sc} + \rho_s [\cos \phi_s - 1]$$

$$r = \rho_s \sin \phi_s$$

Since changes in entropy (and hence total pressure) are assumed to occur only at the shock,  $s$ , a knowledge of the shock shape and all upstream jet flow properties also permits calculating the total pressure of flow after crossing the shock at each point on the shock:

$$P_{Ts} = P_{Th} \left[ \frac{(\gamma+1) M_j^2 \cos^2(\alpha_j - \phi_s)}{(\gamma-1) M_j^2 \cos^2(\alpha_j - \phi_s) + 2} \right]^{\frac{\gamma}{\gamma-1}} \left[ \frac{\gamma+1}{2\gamma M_j^2 \cos^2(\alpha_j - \phi_s) - \gamma + 1} \right]^{\frac{1}{\gamma-1}}$$

Here,  $p_j$ ,  $M_j$ , and  $\alpha_j$  are jet flow properties given as above. These data permit the calculation of the mean total pressure of the layer flow,  $P_{Td}$ , by some sort of averaging technique. In this method an area-weighted average is taken:

$$9. \quad P_{Td} = \frac{\int_0^{\phi_{sd}} P_{Ts} \sin \phi_s \cos(\alpha_j - \phi_s) d\phi_s}{\int_0^{\phi_{sd}} \sin \phi_s \cos(\alpha_j - \phi_s) d\phi_s}$$

Using  $P_{Td}$ ,  $M_d$  and  $P_d$  may be related by the equation:

$$10. \quad P_d = \frac{P_{Td}}{(1 + \frac{\gamma-1}{2} M_d^2)^{\frac{\gamma}{\gamma-1}}}$$

Finally, the mean flow angle at the layer exit,  $\alpha_d$ , may be related to the shock shape and  $\Delta x_d$  if the shape of the flow angle distribution across the layer is assumed. This is because the shock shape, together with the known jet flow field upstream specifies the angle of flow just downstream of the shock at all points along the shock, including at the layer exit:

$$\alpha_{sd} = \alpha_{jd} + \tan^{-1} \left\{ \frac{2 \tan(\alpha_{jd} - \phi_{sd}) [M_{jd}^2 \cos^2(\alpha_{jd} - \phi_{sd}) - 1]}{2 + M_{jd}^2 [\gamma + 1 - 2 \cos^2(\alpha_{jd} - \phi_{sd})]} \right\}$$

(Here  $\alpha_{jd}$ ,  $M_{jd}$  are jet flow properties just upstream of the shock at the intersection of the shock with the jet boundary). Also, the flow angle at the layer exit on the interstage floor,  $\alpha_{fd}$ , must be the same as the angle of the floor itself. Thus, the flow angle at the two ends of the segment  $\Delta x_d$  is specified by the shock shape. In this analysis the flow angle distribution across the layer at  $d$  is assumed linear.



Thus:

$$11. \quad \alpha_d = \frac{1}{2} (\alpha_{sd} + \alpha_{fd})$$

In this method the interstage floor pressure distribution is replaced by an average floor pressure,  $P_f$ , which gives the load on the interstage floor:

$$12. \quad \int_0^{r_d} P_f(r) r dr = P_f r_d^2$$

$$\int_{x_{fc}}^{x_{fd}} P_f(r) r(x) dx = P_f \int_{x_{fc}}^{x_{fd}} r_f(x) dx$$

Furthermore, the layer static pressure distribution is replaced by an average static pressure, which is assumed equal to  $P_f$ :

$$13. \quad \int_0^{r_d} \int_{x_s}^{x_f} P_i(x, r) dx dr = P_f \int_0^{r_d} (x_f - x_s) dr$$

Equations 4 - 13 reduce the number of basic unknowns in equations 1 - 3 to  $\Delta x_d$ ,  $M_d$ , and  $P_f$ . Therefore, there are sufficient basic equations to determine these remaining unknowns. However, the equations are very difficult, due to the term  $(\sin \frac{\Theta}{2})$ . Since  $\Theta$  is arbitrary, it has been convenient to assume it to be a small value, so that  $\sin \frac{\Theta}{2} \approx \frac{\Theta}{2}$ . When this is done,  $\Theta$  divides out of equation 3, and this variable is eliminated from the entire problem.

#### Method of Solution

In this analysis the boundary shape is determined from equations 4 and 5, and the shock centerline standoff is determined from 6, using the given nozzle exit conditions, ambient pressure, and interstage floor shape. The procedure is, next, to enter a  $\Delta x_d$  iteration.  $\Delta x_d$  is assumed, and from this  $r_d$ , the shock shape,  $T_{jr}$ ,  $P_{Td}$ ,  $\alpha_d$ , and the integrals  $\int_0^{r_d} (x_f - x_s) dr$  and  $\int_{x_{fc}}^{x_{fd}} r_f dx$ , are determined. Then, equations 1 - 3, together with 10, are solved for  $p_f$ ,  $M_d$ , and a new  $\Delta x_d$ . The iteration is continued until the assumed and calculated  $\Delta x_d$  agree.

It has been found that this procedure is mathematically very unstable when equations 1-3 are used without modification. For some assumptions of  $\Delta x_d$  there is no solution for  $M_d$ ; for other assumptions a value for  $M_d$  is obtained, but the calculated  $\Delta x_d$  may be negative or imaginary. This behavior has been traced to the term:  $P_f \int_0^{r_d} (x_f - x_s) dr$ . For a range of assumptions of  $\Delta x_d$  which are too small, this term is too small to satisfy equation 3 with flow being out of the stagnation layer at  $d$ , as implied by equations 1 and 11. It has, therefore, been found convenient to increase the size of this term in case the assumed  $\Delta x_d$  is too small, so that the equations become mathematically stable. Consequently, the term:

$$\frac{P_f \phi_{sd}^2 P_s}{4 \cos \phi_{sd} \sin \frac{\phi_{sd}}{2}} (\Delta x_{d \text{ assumed}} - \Delta x_{d \text{ to be calculated}})$$

has been added to  $P_f \int_0^{r_d} (x_f - x_s) dr$  in equation 3. This term compensates for too small a value of  $\Delta x_d(\text{assumed})$ , yet disappears when  $\Delta x_d(\text{assumed})$  approaches the calculated value. The form of this term arises from a consideration of the effect of an error in  $\Delta x_d$  on the layer area,  $\int_0^{r_d} (x_f - x_s) dr$ .

Eliminating  $P_d$ ,  $P_f$ , and  $\Delta x_d(\text{calculated})$  from equations 1, 2, 10, and the modified equation 3, we have:

$$\begin{aligned} 14. \quad P_d &= \frac{P_{Td}}{(1 + \frac{\gamma-1}{2} M_d^2)^{\frac{\gamma}{\gamma-1}}} \\ &= \frac{\frac{C_c K}{r_d \sin \alpha_d} (C_x + P_d r_d^2 - \frac{2\gamma C_c \cos \alpha_d M_d}{\sqrt{1 + \frac{\gamma-1}{2} M_d^2}})}{\frac{C_c r_d^2}{\sin \alpha_d} (1 + \gamma M_d^2 \sin^2 \alpha_d) - M_d \sqrt{1 + \frac{\gamma-1}{2} M_d^2} \left[ \frac{1}{2} r_d^2 + (C_x + P_d r_d^2 - \frac{2\gamma C_c \cos \alpha_d M_d}{\sqrt{1 + \frac{\gamma-1}{2} M_d^2}}) (A_{fr} + A_1 - K \Delta x_d) \right]} \end{aligned}$$

$$\begin{aligned} \text{where: } C_c &= \frac{P_{Tn} r_n^2}{2 \left( \frac{\gamma+1}{2} \right)^{\frac{\gamma+1}{\gamma-1}}} ; \quad A_{fr} = \int_{x_{fc}}^{x_{fd}} r_f dx ; \\ C_x &= r_n^2 \left[ \frac{(1 + \gamma M_n^2) P_{Tn}}{(1 + \frac{\gamma-1}{2} M_n^2)^{\frac{\gamma}{\gamma-1}}} - P_d \right] ; \quad A_1 = \int_0^{r_d} (x_f - x_s) dr ; \\ K &= \frac{\phi_{sd}^2 P_s}{4 \cos \phi_{sd} \sin \frac{\phi_{sd}}{2}} ; \quad \Delta x_{d \text{ cal}} = \Delta x_{d \text{ assumed}} \end{aligned}$$

Within each  $\Delta x_d$  iteration, equation 14 is used to solve for  $M_d$ .  $P_d$  as calculated from both expressions of 14 is forced to be the same by trial and error adjustment of  $M_d$ . When a value of  $M_d$  for the iteration has been found, a calculated  $\Delta x_d$  is obtained from equation 1:

$$1. \quad \Delta x_d = \frac{C_c}{P_d r_d \sin \alpha_d M_d \sqrt{1 + \frac{r-1}{2} M_d^2}}$$

When the  $\Delta x_d$  iteration has converged,  $P_f$  is calculated by:

$$P_f = \frac{\sqrt{1 + \frac{r-1}{2} M_d^2} (C_x + P_d r_d^2) - 2 \gamma C_c \cos \alpha_d M_d}{r_d^2 \sqrt{1 + \frac{r-1}{2} M_d^2}},$$

and the total load on the interstage floor is given by:

$$L = \pi r_d^2 P_f$$

APPENDIX II

EXPERIMENTAL DATA

### Explanation

The data presented herein is divided into two broad classifications, sonic nozzle configurations and supersonic nozzle configurations. The pressure data is normalized to a nozzle total pressure of 1900 psia. To make use of the pressure data for a different total pressure, multiply the pressure data by the new total pressure times  $10^{-3}$ . The force ratios can be used directly.

All the data presented was taken at the same value of nozzle total pressure to ambient pressure ratio,  $1.2 \times 10^4$ . For "closed" configurations, that is, configurations having a nozzle plate and/or a circular fence, the local ambient pressure is not the same as the ambient, or test cell, pressure. In particular, for configurations having a nozzle plate, the local ambient pressure is, in general, vastly different from the test cell pressure. This local ambient pressure, which determines the shape and extent of the jet boundary, is essentially unknown. Hence, the pressure ratio mentioned above is based on the test cell pressure.

The circular fence used throughout the test had a height of 21.7 exit radii for the sonic nozzle, and 9.07 exit radii for the supersonic nozzle. The inside diameter of the fence, the base plate diameter and the nozzle plate diameter were all 86.8 exit radii for the sonic nozzle, and 36.28 exit radii for the supersonic nozzle.

The locations of the pressure probes used in the test are indicated on the plots of rake pressures. The symbols  $H$ ,  $R_R$ , and  $\gamma$ , used to locate the probes, are defined as in Figure (6), as are all other symbols encountered in the plots.

### Summary of the Data

$$P_{Tn} = 1000 \text{ psia} \qquad P_{Tn}/P_a = 12000 \qquad \gamma = 1.4$$

Supersonic Nozzle:

$$A/A^* = 5.5 \qquad \alpha_n = 16^\circ$$

Sonic Nozzle:

$$A/A^* = 1.0 \qquad \alpha_n = 0^\circ$$

- Figure 1                      Sonic Nozzle                      Flat Plate
- Plate Pressure Distribution
  - Plate Force/Thrust Ratio and Rake Pressures vs Separation Distance
- Figure 2                      Sonic Nozzle                      Flat Plate with Nozzle Plate
- Plate Pressure Distribution
  - Plate Force/Thrust Ratio and Rake Pressures vs Separation Distance
  - Nozzle Plate Force/Thrust Ratio vs Separation Distance and Nozzle Plate Pressure Distribution
- Figure 3                      Sonic Nozzle                      Flat Plate with Circular Fence ( $h/r_n = 0$ )
- Plate Pressure Distribution
  - Fence Pressure Distribution
  - Plate Force/Thrust Ratio and Rake Pressures vs Separation Distance
- Figure 4                      Sonic Nozzle                      Flat Plate with Nozzle Plate and Circular Fence ( $h/r_n = 0$ )
- Plate Pressure Distribution
  - Fence Pressure Distribution
  - Plate Force/Thrust Ratio and Rake Pressures vs Separation Distance
  - Nozzle Plate Force/Thrust Ratio vs Separation Distance and Nozzle Plate Pressure Distribution
- Figure 5                      Sonic Nozzle                      Flat Plate with Circular Fence ( $h/r_n = 10.90$ )
- Plate Pressure Distribution
  - Fence Pressure Distribution
  - Plate Force/Thrust Ratio and Rake Pressures vs Separation Distance

Figure 6                      Sonic Nozzle                      Flat Plate with Nozzle Plate and  
Circular Fence (  $h/r_n = 10.98$  )

- a. Plate Pressure Distribution
- b. Fence Pressure Distribution
- c. Plate Force/Thrust Ratio and Rake Pressures vs Separation Distance
- d. Nozzle Plate Force/Thrust Ratio vs Separation Distance and Nozzle Plate Pressure Distribution

Figure 7                      Sonic Nozzle                      Flat Plate with Circular Fence (  $h/r_n = 16.30$  )

- a. Plate Pressure Distribution
- b. Fence Pressure Distribution
- c. Plate Force/Thrust Ratio and Rake Pressures vs Separation Distance

Figure 8                      Sonic Nozzle                      Flat Plate with Circular Fence (  $h/r_n = 21.70$  )

- a. Plate Pressure Distribution
- b. Fence Pressure Distribution
- c. Plate Force/Thrust Ratio and Rake Pressures vs Separation Distance

Figure 9                      Sonic Nozzle                      Simulated Re-entry Body Flare

- a. Plate Pressure Distribution
- b. Fence Pressure Distribution
- c. Plate Force/Thrust Ratio and Rake Pressures vs Separation Distance
- d. Nozzle Plate Force/Thrust Ratio vs Separation Distance and Nozzle Plate Pressure Distribution

- Figure 10      Sonic Nozzle      Flat Plate with Nozzle Tilted  $4.7^\circ$  and  $9.8^\circ$
- Plate Pressure Distribution - Plane 1
  - Plate Pressure Distribution - Plane 2
  - Plate Pressure Distribution - Plane 3
  - Plate Force/Thrust Ratio and Rake Pressures vs Separation Distance -  $4.7^\circ$
  - Plate Force Thrust Ratio and Rake Pressures vs. Separation Distance -  $9.8^\circ$
- Figure 11      Sonic Nozzle      Cone, Altitude = 21.7 radii
- Plate Pressure Distribution
  - Plate Force/Thrust Ratio and Rake Pressures vs Separation Distance
- Figure 12      Supersonic Nozzle      Flat Plate
- Plate Pressure Distribution
  - Plate Force/Thrust Ratio and Rake Pressures vs Separation Distance
- Figure 13      Supersonic Nozzle      Flat Plate with Nozzle Plate
- Plate Pressure Distribution
  - Plate Force/Thrust Ratio and Rake Pressures vs Separation Distance
  - Nozzle Plate Force/Thrust Ratio vs Separation Distance and Nozzle Plate Pressure Distribution
- Figure 14      Supersonic Nozzle      Flat Plate with Circular Fence ( $h/r_n = 0$ )
- Plate Pressure Distribution
  - Fence Pressure Distribution
  - Plate Force/Thrust Ratio and Rake Pressures vs Separation Distance



Figure 15

Supersonic Nozzle      Flat Plate with Nozzle Plate and  
Circular Fence (  $h/r_n = 0$  )

- a. Plate Pressure Distribution
- b. Fence Pressure Distribution
- c. Plate Force/Thrust Ratio and Rake Pressures vs Separation
- d. Nozzle Plate Force/Thrust Ratio vs Separation Distance and Nozzle Plate Pressure Distribution

Figure 16

Supersonic Nozzle      Flat Plate with Nozzle Plate and  
Circular Fence (  $h/r_n = 1.134$  )

- a. Plate Pressure Distribution
- b. Fence Pressure Distribution
- c. Plate Force/Thrust Ratio and Rake Pressure vs Separation Distance
- d. Nozzle Plate Force/Thrust Ratio vs Separation Distance and Nozzle Plate Pressure Distribution

Figure 17

Supersonic Nozzle      Flat Plate with Circular Fence (  $h/r_n = 2.268$  )

- a. Plate Pressure Distribution
- b. Fence Pressure Distribution
- c. Plate Force/Thrust Ratio and Rake Pressures vs Separation Distance

Figure 18

Supersonic Nozzle      Flat Plate with Nozzle Plate and Circular  
Fence (  $h/r_n = 2.268$  )

- a. Plate Pressure Distribution
- b. Fence Pressure Distribution
- c. Plate Force/Thrust Ratio and Rake Pressures vs Separation Distance
- d. Nozzle Plate Force/Thrust Ratio vs Separation Distance and Nozzle Plate Pressure Distribution

- Figure 19      Supersonic Nozzle      Flat Plate with Circular Fence (  $h/r_n = 4.535$  )
- Plate Pressure Distribution
  - Fence Pressure Distribution
  - Plate Force/Thrust Ratio and Rake Pressures vs Separation Distance
- Figure 20      Supersonic Nozzle      Flat Plate with Nozzle Plate and Circular Fence (  $h/r_n = 4.535$  )
- Plate Pressure Distribution
  - Fence Pressure Distribution
  - Plate Force/Thrust Ratio and Rake Pressures vs Separation Distance
  - Nozzle Plate Force/Thrust Ratio vs Separation Distance and Nozzle Plate Pressure Distribution
- Figure 21      Supersonic Nozzle      Flat Plate with Nozzle Plate and Nozzle Tilted  $10^\circ$
- Plate Pressure Distribution - Plane 1
  - Plate Pressure Distribution - Plane 2
  - Plate Pressure Distribution - Plane 3
  - Plate Force/Thrust Ratio and Rake Pressures vs Separation Distance
  - Nozzle Plate Force/Thrust Ratio vs Separation Distance and Nozzle Plate Pressure Distribution
- Figure 22      Supersonic Nozzle      Flat Plate with Nozzle Plate and Circular Fence (  $h/r_n = 0$  ) Nozzle Tilted  $10^\circ$
- Plate Pressure Distribution - Plane 1
  - Plate Pressure Distribution - Plane 2
  - Plate Pressure Distribution - Plane 3
  - Fence Pressure Distribution
  - Plate Force/Thrust Ratio and Rake Pressures vs Separation Distance
  - Nozzle Plate Force/Thrust Ratio vs Separation Distance and Nozzle Plate Pressure Distribution